Published by Institute of Physics Publishing for SISSA

Received: *June 25, 2007*
Revised: *August 16, 2007*
Accepted: *December 20, 2007*
Published: *January 8, 2008*

Non-perturbative renormalization of the static vector current and its $\mathrm{O}(a)$-improvement in quenched QCD

ALPHA Collaboration

Filippo Palombi

DESY, Theory Group, Platanenallee 6, D-15738 Zeuthen, Germany
E-mail: filippo.palombi@desy.de

Abstract: We carry out the renormalization and the Symanzik $\mathrm{O}(a)$-improvement programme for the static vector current in quenched lattice QCD. The scale independent ratio of the renormalization constants of the static vector and axial currents is obtained non-perturbatively from an axial Ward identity with Wilson-type light quarks and various lattice discretizations of the static action. The improvement coefficients $c_{\mathrm{V}}^{\mathrm{stat}}$ and $b_{\mathrm{V}}^{\mathrm{stat}}$ are obtained up to $\mathrm{O}(g_0^4)$-terms by enforcing improvement conditions respectively on the axial Ward identity and a three-point correlator of the static vector current. A comparison between the non-perturbative estimates and the corresponding one-loop results shows a non-negligible effect of the $\mathrm{O}(g_0^4)$-terms on the improvement coefficients but a good accuracy of the perturbative description of the ratio of the renormalization constants.

Keywords: Lattice Quantum Field Theory, Lattice Gauge Field Theories, Lattice QCD.

JHEP01(2008)021

Contents

JHEP01(2008)021

1. Introduction

Semileptonic decays of B-mesons constitute a very important source of experimental information in B-physics. They have been and are currently being investigated as a part of the research programmes of BaBar [1] and CLEO [2]. The prototype for such decays is $B^0 \to \pi^- \ell^+ \nu$. Once the amplitude of this process is known, an experimental measurement of its branching ratio allows in principle to extract the CKM matrix element $|V_{ub}|$. From a theoretical point of view, the transition is mediated by the heavy-light vector current, and the problem of knowing the decay amplitude amounts to calculating the QCD matrix element

$$\langle \pi(p)|V_\mu|B(k)\rangle = \left(k + p - q\frac{m_B^2 - m_\pi^2}{q^2}\right)_\mu f_+(q^2) + \frac{m_B^2 - m_\pi^2}{q^2} q_\mu f_0(q^2)\,, \tag{1.1}$$

or equivalently the form factors $f_{+/0}(q^2)$, with $q = k - p$ the 4-momentum transferred from the B-meson to the pion.

Given the large mass of the b-quark, a direct lattice calculation of eq. (1.1) requires tiny lattice spacings ($a \ll 1/(5\mathrm{GeV})$) and big volumes ($L > 1.5$ fm) in order to correctly reproduce the quark dynamics without squeezing the B-meson at reasonably small light-quark masses. Various solutions have been proposed to overcome this difficulty: the reader is referred to [3, 4] for recent reviews. Among these we mention the Heavy Quark Effective Theory (HQET) and the Step Scaling Method (SSM).

In HQET eq. (1.1) is expanded in inverse powers of the b-quark mass. The leading contribution, also known as the static approximation, describes the heavy quark in terms of a renormalizable effective field theory. Although lattice simulations in the original formulation [5] were hampered by large statistical fluctuations due to self-energy effects of the heavy propagator, thanks to the recent introduction of new lattice regularizations [6] it is now possible to simulate static quarks with much improved numerical precision.

The SSM, a relativistic technique based on finite size scaling, has been proposed some years ago by the *Tor Vergata group* in relation to a study of the heavy-light decay constants [7] and meson masses [8]. It has been recently shown in [9] that combining the SSM with HQET enables a strict control of the mass extrapolations and a consequent reduction of the corresponding systematic uncertainties.

From this point of view it would be of considerable interest to extend the combined approach "HQET + SSM" to eq. (1.1), since a first attempt to apply the *Tor Vergata* method to the form factors has been recently presented in [10]. The goal is ambitious in that observables such as eq. (1.1) are intrinsically more complex than a decay constant or a meson mass, owing to the appearance of an additional mass scale to be identified with q^2.

In this paper we concentrate on HQET. In view of a non-perturbative computation of eq. (1.1), the static vector current must first be non-perturbatively renormalized. This task has been partially accomplished, since in the static approximation the spatial components $V_k^{\rm stat}$ are renormalized by the same renormalization constant $Z_{\rm A}^{\rm stat}$ as the temporal component of the static axial current $A_0^{\rm stat}$. The Renormalization Group (RG) running of the latter has been computed both in the quenched approximation [11] and with two dynamical quarks [12]. In order to compute the renormalization constant $Z_{\rm V}^{\rm stat}$ of the temporal component of the static vector current $V_0^{\rm stat}$, we derive an axial Ward identity (WI), much in the spirit of [13, 14], relating $Z_{\rm V}^{\rm stat}$ to $Z_{\rm A}^{\rm stat}$. The scale independent ratio $Z_{\rm A}^{\rm stat}/Z_{\rm V}^{\rm stat}$ is then computed through an explicit implementation of the WI in the Schrödinger functional (SF) at the chiral point. On-shell $\mathrm{O}(a)$-improvement at zero light-quark mass is obtained by adding a single counter-term to the static vector current, proportional to the improvement coefficient $c_{\rm V}^{\rm stat}$, which is then tuned according to the request that the axial WI be satisfied at finite lattice spacing up to $\mathrm{O}(a^2)$-terms.

The improvement of the static vector current $V_0^{\rm stat}$ at non-zero light-quark mass, realized in principle through the introduction of a second improvement coefficient $b_{\rm V}^{\rm stat}$, is not easily achievable in terms of the WI, which takes its simplest form in the chiral limit. For this reason, we adopt a different improvement condition, i.e we obtain $b_{\rm V}^{\rm stat}$ by imposing that the ratio of a three-point SF correlator of the static vector current at zero and non-zero light-quark mass be the same in two different static regularizations up to $\mathrm{O}(a^2)$-terms, thus determining the difference $\Delta b_{\rm V}^{\rm stat}$ corresponding to the chosen actions. This procedure repeats the one adopted in [6] for the determination of $b_{\rm A}^{\rm stat}$. In order to isolate the value of $b_{\rm V}^{\rm stat}$ corresponding to all the static discretizations, the knowledge of $b_{\rm V}^{\rm stat}$ is required for at least one of them. This is a difficult problem, which we solve only approximately by computing $b_{\rm V}^{\rm stat}$ at one-loop order in perturbation theory for the static actions with the simplest lattice Feynman rules, i.e. the Eichten-Hill (EH) and the APE ones. This somewhat unsatisfactory solution introduces $\mathrm{O}(g_0^4)$ systematic uncertainties,

JHEP01(2008)021

which are discussed in detail.

Other appealing applications where the static vector current plays a rôle can be found within the domain of twisted mass QCD [15, 16], where the static axial current acquires a vector component after a twist rotation of the light-quark fields. This is the case, for instance, with the computation of $B_B^{\rm stat}$, for which the matrix elements of the $\Delta B = 2$ four-fermion operators have to be normalized by appropriate bilinear correlators of the static axial current [17].

The paper is organized as follows. The axial WI is derived in section 2, where the notation is also established. Its implementation in the framework of the SF is discussed in section 3. Section 4 is devoted to a one-loop perturbative analysis of the lattice artefacts in various WI topologies. In section 5 we present our non-perturbative results for the improvement coefficient $c_{\rm V}^{\rm stat}$ and the O(a)-improved ratio $Z_{\rm A}^{\rm stat}/Z_{\rm V}^{\rm stat}$, and in section 6 we discuss the improvement coefficient $b_{\rm V}^{\rm stat}$. Conclusions are drawn in section 7. Additional tables containing perturbative and non-perturbative results have been collected in appendix A.

2. Formal derivation of the axial WI

As for the theoretical derivation of the axial WI, we follow the approach of [18, 19]. For the moment no attention is paid to the specific regularization of the theory. We assume a fermion content with an isospin doublet of degenerate light-quarks $\psi^T = (\psi_1, \psi_2)$ and a single heavy-quark, described by a pair of static fields $(\psi_{\rm h}, \psi_{\bar{\rm h}})$. In order to set up the notation, we introduce the light-quark isovector axial and vector currents and the pseudoscalar density

$$A_\mu^a(x) = \bar{\psi}(x)\gamma_\mu\gamma_5\frac{1}{2}\tau^a\psi(x)\,, \tag{2.1}$$

$$V_\mu^a(x) = \bar{\psi}(x)\gamma_\mu\frac{1}{2}\tau^a\psi(x)\,, \tag{2.2}$$

$$P^a(x) = \bar{\psi}(x)\gamma_5\frac{1}{2}\tau^a\psi(x)\,, \tag{2.3}$$

as well as their heavy-light companions (for which we explicitly indicate light-quark flavour indices)

$$A_\mu^{k\rm h}(x) = \bar{\psi}_k(x)\gamma_\mu\gamma_5\psi_{\rm h}(x), \tag{2.4}$$

$$V_\mu^{k\rm h}(x) = \bar{\psi}_k(x)\gamma_\mu\psi_{\rm h}(x), \tag{2.5}$$

$$P^{{\rm h}k}(x) = \bar{\psi}_{\rm h}(x)\gamma_5\psi_k(x)\,, \qquad k = 1, 2\;. \tag{2.6}$$

The general WI follows from the invariance of the path integral representation of correlation functions under chiral rotations of the light-quark fields. In particular, we consider an axial variation

$$\delta_{\rm A}^a\psi(x) = \omega^a(x)\frac{1}{2}\tau^a\gamma_5\psi(x)\,, \qquad \delta_{\rm A}^a\bar{\psi}(x) = \omega^a(x)\bar{\psi}(x)\gamma_5\frac{1}{2}\tau^a\,, \tag{2.7}$$

where τ^a denotes a Pauli matrix acting on the isospin space and $\omega^a(x)$ is a smooth function which vanishes outside some bounded region R. Since the Pauli matrices are traceless,

JHEP01(2008)021

the functional integration measure is invariant under eq. (2.7) and we conclude that the correlation function of a given operator $\mathcal{O}$ satisfies the equation

$$\langle \mathcal{O}\delta_{\mathrm{A}}^{a} S\rangle = \langle \delta_{\mathrm{A}}^{a}\mathcal{O}\rangle \,, \tag{2.8}$$

where

$$\delta_{\mathrm{A}}^{a} S = \int_R \mathrm{d}^4x \; \omega^a(x) \left\{ -\partial_\mu A_\mu^a(x) + 2mP^a(x) \right\} \tag{2.9}$$

represents the axial variation of the light-quark action and m denotes the PCAC quark mass. We assume in what follows that $\mathcal{O}$ factorizes into the product of two operators $\mathcal{O}_{\mathrm{int}}$ and $\mathcal{O}_{\mathrm{ext}}$, polynomials in the basic fields and localized in the interior and exterior of R respectively. Accordingly, eq. (2.8) reads

$$\langle \mathcal{O}_{\mathrm{int}}\mathcal{O}_{\mathrm{ext}}\delta_{\mathrm{A}}^{a} S\rangle = \langle \mathcal{O}_{\mathrm{ext}}\delta_{\mathrm{A}}^{a}\mathcal{O}_{\mathrm{int}}\rangle \;. \tag{2.10}$$

We now concentrate on the isovector component $a = 1$. In our specific application we choose $\mathcal{O}_{\mathrm{int}}(x) = V_0^{1\mathrm{h}}(x)$ for $x \in R$ and $\mathcal{O}_{\mathrm{ext}}(y) = P^{\mathrm{h}2}(y)$ for $y \notin R$, thus obtaining

$$\langle A_0^{2\mathrm{h}}(x)P^{\mathrm{h}2}(y)\rangle = 2\langle V_0^{1\mathrm{h}}(x)P^{\mathrm{h}2}(y)\int_R \mathrm{d}^4z \left\{ \partial_\mu A_\mu^1 - 2mP^1 \right\}\rangle \;. \tag{2.11}$$

If we further require R to be a time-oriented cylinder with periodic b.c. in space, i.e.

$$R = \{x: \; t_1 \le x_0 \le t_2\}, \tag{2.12}$$

we immediately see that the space derivatives of the light axial current on the right hand side of eq. (2.11) drop out, while the temporal derivative gives rise to a boundary contribution. After a space integration of both sides over $\mathbf{x}$, we arrive at our final expression

$$\langle Q_{\mathrm{A}}^{2\mathrm{h}}(x_0)P^{\mathrm{h}2}(y)\rangle = 2\langle Q_{\mathrm{V}}^{1\mathrm{h}}(x_0)P^{\mathrm{h}2}(y)\left\{ \left[Q_{\mathrm{A}}^1(t_2) - Q_{\mathrm{A}}^1(t_1)\right] - 2m\int_R \mathrm{d}^4z P^1(z)\right\}\rangle \,, \tag{2.13}$$

where $x_0 \in [t_1, t_2]$, $y_0 \notin [t_1, t_2]$ and we have introduced the axial and vector charges

$$Q_{\mathrm{A}}^a(x_0) = \int \mathrm{d}^3\mathbf{x} \; A_0^a(x) \,, \tag{2.14}$$

$$Q_{\mathrm{A}}^{k\mathrm{h}}(x_0) = \int \mathrm{d}^3\mathbf{x} \; A_0^{k\mathrm{h}}(x) \,, \tag{2.15}$$

$$Q_{\mathrm{V}}^{k\mathrm{h}}(x_0) = \int \mathrm{d}^3\mathbf{x} \; V_0^{k\mathrm{h}}(x) \;. \tag{2.16}$$

eq. (2.13) has to be understood as a relation among renormalized quantities. It should be observed that Q_{A}^1 and P^1 consist of two contributions in the flavour space, corresponding to the non-zero matrix elements of τ^1. Out of them, only those with flavour content $\bar\psi_2\psi_1$ contribute to the right hand side of the WI. These will be denoted respectively Q_{A}^{21} and P^{21}.

JHEP01(2008)021

3. Lattice implementation in the SF

The axial WI admits a straightforward lattice implementation. We adopt here a SF topology where periodic boundary conditions (up to a phase θ for the light-quark fields) are set up on the spatial directions and Dirichlet boundary conditions are imposed on time at $x_0 = 0, T$. For a discussion of the original application of the SF to the simplest WI, namely the PCAC, we refer the reader to [20]. Unexplained notation closely follows [21].

Although the SF is formally defined in the continuum, we find it convenient to work at finite lattice spacing. Light quarks are assumed to be described by the O(a)-improved Wilson action, with the usual Sheikholeslami-Wohlert term in the bulk and boundary counter-terms proportional to the improvement coefficients $c_{\rm t}-1$ and $\tilde{c}_{\rm t}-1$. No background field is assumed. The static quark is instead defined in terms of the action

$$S_{\rm W}^{\rm stat}[\psi_h,\bar{\psi}_h,\psi_{\bar{h}},\bar{\psi}_{\bar{h}},U] = a^4\sum_x \left[\bar{\psi}_h(x)D_0^{{\rm W}*}\psi_h(x) - \bar{\psi}_{\bar{h}}(x)D_0^{\rm W}\psi_{\bar{h}}(x)\right] , \tag{3.1}$$

where the forward and backward covariant derivatives

$$\begin{aligned} D_0^{\rm W}\psi(x) &= \frac{1}{a}\left[W(x,0)\psi(x+a\hat{0}) - \psi(x)\right] , \\ D_0^{{\rm W}*}\psi(x) &= \frac{1}{a}\left[\psi(x) - W^{\dagger}(x-a\hat{0},0)\psi(x-a\hat{0})\right] , \end{aligned} \tag{3.2}$$

depend upon a parallel transporter W, which can be variously defined. In this paper we consider four possible versions, namely EH, APE, HYP1 and HYP2, respectively corresponding to

$$\begin{aligned} W^{\rm EH}(x,0) &= U(x,0)\,, \\ W^{\rm APE}(x,0) &= V(x,0)\,, \\ W^{\rm HYP1}(x,0) &= V_{\vec{\alpha}}^{\rm HYP}(x,0)\big|_{\vec{\alpha}=(0.75,0.6,0.3)}\,, \\ W^{\rm HYP2}(x,0) &= V_{\vec{\alpha}}^{\rm HYP}(x,0)\big|_{\vec{\alpha}=(1.0,1.0,0.5)}\,. \end{aligned} \tag{3.3}$$

In the above definitions $V(x,0)$ represents the average of the six staples surrounding the gauge link $U(x,0)$, while $V^{\rm HYP}(x,0)$ denotes the temporal HYP link of [22], with the approximate $SU(3)$ projection of [6].

In order to translate eq. (2.13) into the language of the SF, we insert the static vector current in the middle of the bulk, i.e. at $x_0 = T/2$. The support region R is then defined by localizing t_1 and t_2 at different points, with the understanding that $0 < t_1 < x_0 < t_2 < T$ in order to avoid possible contact terms. The pseudoscalar density is replaced by a boundary source uniformly distributed over the spatial coordinates, i.e.

$$\Sigma^{\rm h2} = \frac{a^6}{L^3}\sum_{\mathbf{yz}} \bar{\zeta}_{\rm h}(\mathbf{y})\gamma_5\zeta_2(\mathbf{z}) . \tag{3.4}$$

On-shell O(a)-improvement of the quark currents requires the introduction of operator counter-terms, whose structure has been discussed in [20, 23]. Accordingly, we introduce the O(a)-improved currents

$$A_0^{ij;\mathrm{I}}(x) = A_0^{ij}(x) + ac_{\mathrm{A}}\delta A_0^{ij}(x)\,, \qquad \delta A_0^{ij}(x) = \frac{1}{2}(\partial_0 + \partial_0^*)\bar{\psi}_i(x)\gamma_5\psi_j(x)\;; \tag{3.5}$$

$$A_0^{k\mathrm{h};\mathrm{I}}(x) = A_0^{k\mathrm{h}}(x) + ac_{\mathrm{A}}^{\mathrm{stat}}\delta A_0^{k\mathrm{h}}(x)\,, \qquad \delta A_0^{k\mathrm{h}}(x) = \bar{\psi}_k(x)\gamma_j\gamma_5\frac{1}{2}(\overleftarrow{\nabla}_j + \overleftarrow{\nabla}_j^*)\psi_{\mathrm{h}}(x)\;; \tag{3.6}$$

$$V_0^{k\mathrm{h};\mathrm{I}}(x) = V_0^{k\mathrm{h}}(x) + ac_{\mathrm{V}}^{\mathrm{stat}}\delta V_0^{k\mathrm{h}}(x)\,, \qquad \delta V_0^{k\mathrm{h}}(x) = \bar{\psi}_k(x)\gamma_j\frac{1}{2}(\overleftarrow{\nabla}_j + \overleftarrow{\nabla}_j^*)\psi_{\mathrm{h}}(x)\;; \tag{3.7}$$

and the O(a)-improved charges

$$Q_{\mathrm{A}}^{ij;\mathrm{I}}(x_0) = a^3\sum_{\mathbf{x}} A_0^{ij;\mathrm{I}}(x) \;= Q_{\mathrm{A}}^{ij}(x_0) + ac_{\mathrm{A}}\delta Q_{\mathrm{A}}^{ij}(x_0)\,, \tag{3.8}$$

$$Q_{\mathrm{A}}^{k\mathrm{h};\mathrm{I}}(x_0) = a^3\sum_{\mathbf{x}} A_0^{k\mathrm{h};\mathrm{I}}(x) = Q_{\mathrm{A}}^{k\mathrm{h}}(x_0) + ac_{\mathrm{A}}^{\mathrm{stat}}\delta Q_{\mathrm{A}}^{k\mathrm{h}}(x_0)\,, \tag{3.9}$$

$$Q_{\mathrm{V}}^{k\mathrm{h};\mathrm{I}}(x_0) = a^3\sum_{\mathbf{x}} V_0^{k\mathrm{h};\mathrm{I}}(x) = Q_{\mathrm{V}}^{k\mathrm{h}}(x_0) + ac_{\mathrm{V}}^{\mathrm{stat}}\delta Q_{\mathrm{V}}^{k\mathrm{h}}(x_0)\,, \tag{3.10}$$

where, as also explained at the end of last section, the notation $\mathcal{O}^{ij}$ always refers to a flavour content $\bar{\psi}_i\psi_j$. The improvement coefficients c_{A}, $c_{\mathrm{A}}^{\mathrm{stat}}$ and $c_{\mathrm{V}}^{\mathrm{stat}}$ depend on the gauge coupling and are perturbatively expanded according to

$$c = c^{(1)}g_0^2 + c^{(2)}g_0^4 + \mathrm{O}(g_0^6)\;. \tag{3.11}$$

In view of phenomenological applications, it is useful to allow for renormalized currents at non-zero light-quark mass. O(a)-improvement requires in this case the introduction of additional mass counter-terms, proportional to $m_{\mathrm{q}} = m - m_{\mathrm{cr}}$. The relations between renormalized currents and their bare counterparts explicitly read

$$\begin{aligned} A_{0,\mathrm{R}}^{ij;\mathrm{I}}(x) &= Z_{\mathrm{A}}[1 + b_{\mathrm{A}}am_{\mathrm{q}}]A_0^{ij;\mathrm{I}}(x)\,, \\ A_{0,\mathrm{R}}^{k\mathrm{h};\mathrm{I}}(x) &= Z_{\mathrm{A}}^{\mathrm{stat}}[1 + b_{\mathrm{A}}^{\mathrm{stat}}am_{\mathrm{q}}]A_0^{k\mathrm{h};\mathrm{I}}(x)\,, \\ V_{0,\mathrm{R}}^{k\mathrm{h};\mathrm{I}}(x) &= Z_{\mathrm{V}}^{\mathrm{stat}}[1 + b_{\mathrm{V}}^{\mathrm{stat}}am_{\mathrm{q}}]V_0^{k\mathrm{h};\mathrm{I}}(x)\;. \end{aligned} \tag{3.12}$$

The SF implementation of the axial WI is then realized through the introduction of a set of two- and three-point correlation functions,

$$\begin{aligned} h_{\mathrm{A}}^{\mathrm{I}}(x_0) &= \langle Q_{\mathrm{A}}^{2\mathrm{h};\mathrm{I}}(x_0)\Sigma^{\mathrm{h}2}\rangle\,, \\ h_{\mathrm{VA}}^{\mathrm{I}}(x_0,y_0) &= \langle Q_{\mathrm{V}}^{1\mathrm{h};\mathrm{I}}(x_0)Q_{\mathrm{A}}^{21;\mathrm{I}}(y_0)\Sigma^{\mathrm{h}2}\rangle\,, \\ h_{\mathrm{VP}}^{\mathrm{I}}(x_0,y_0) &= \frac{a^3}{L^3}\sum_{\mathbf{y}}\langle Q_{\mathrm{V}}^{1\mathrm{h};\mathrm{I}}(x_0)P^{21}(y)\Sigma^{\mathrm{h}2}\rangle\,, \end{aligned} \tag{3.13}$$

which are graphically represented by the Feynman diagrams of figure 1. It should be observed that the two-point correlator $h_{\mathrm{A}}^{\mathrm{I}}$ satisfies the relation $h_{\mathrm{A}}^{\mathrm{I}} = -2f_{\mathrm{A}}^{\mathrm{stat,I}}$ with $f_{\mathrm{A}}^{\mathrm{stat,I}}$ defined in eqs. (3.22-3.24) of [23]. Once the renormalized currents are expressed in terms of

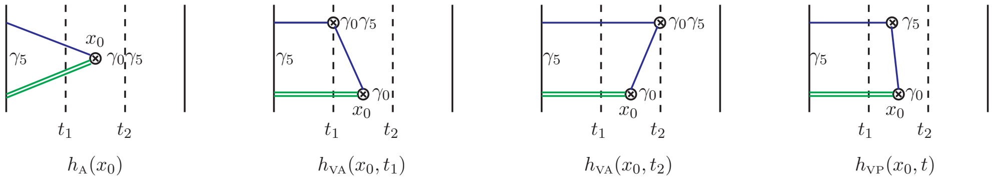

Figure 1: Diagrammatic representation of the SF correlation functions of eq. (3.13). A single (double) line describes the propagation of a light (static) quark.

$\mathcal{T}$	T/L	x_0/T	t_1/T	t_2/T
1	1	1/2	1/4	3/4
2	2	1/2	1/4	3/4
3	3/2	1/2	1/3	2/3
4	3	1/2	1/3	2/3

Table 1: Some topologies $\mathcal{T}$ of the WI.

the bare ones, the axial WI takes the form of a constraining relation among renormalization constants. In the chiral limit it reduces to

$$\mathcal{R} \equiv \frac{h^{\mathrm{I}}_{\mathrm{VA}}(x_0,t_2) - h^{\mathrm{I}}_{\mathrm{VA}}(x_0,t_1)}{h^{\mathrm{I}}_{\mathrm{A}}(x_0)} = \frac{Z^{\mathrm{stat}}_{\mathrm{A}}}{Z^{\mathrm{stat}}_{\mathrm{V}} Z_{\mathrm{A}}} + \mathrm{O}(a^2) \ . \tag{3.14}$$

In order to pursue a numerical implementation of eq. (3.14), some geometrical parameters have to be specified, namely the ratios T/L, t_1/T, t_2/T and the θ-angle of the SF. Concerning the latter, we consider three possible values, i.e. $\theta = 0.0, 0.5, 1.0$. The other parameters will instead be collectively referred to as the topology $\mathcal{T}$ of the WI. In table 1 we list four possibilities. Each of them affects the noise-to-signal ratio of the non-perturbative simulations in its own way and introduces specific cutoff effects in the ratio $\mathcal{R}$ at finite lattice spacing. Therefore, a convenient choice of $\mathcal{T}$ imposes — at least theoretically – a balance between the minimization of the lattice artefacts and the maximization of the numerical signal.

We remark that eq. (3.14), which we use in order to determine $c^{\mathrm{stat}}_{\mathrm{V}}$, depends as well on the improvement coefficients c_{A} and $c^{\mathrm{stat}}_{\mathrm{A}}$. These have been determined respectively in [24] and [6] and are taken as input parameters here. In particular, $c^{\mathrm{stat}}_{\mathrm{A}}$ is analytically known at one-loop order for the EH and APE actions, and effectively up to $\mathrm{O}(g_0^4)$-terms for the HYP1 and HYP2 actions. Scaling tests of $c^{\mathrm{stat}}_{\mathrm{A}}$ have been extensively discussed in [6], to which the reader is referred for details. Here we stress that the lack of a full knowledge of $c^{\mathrm{stat}}_{\mathrm{A}}$ introduces systematic uncertainties at order $\mathrm{O}(g_0^4)$ in the determination of $c^{\mathrm{stat}}_{\mathrm{V}}$. On the other hand, the WI is independent of the boundary improvement coefficients c_{t} and $\tilde{c}_{\mathrm{t}}$. This has been explicitely checked in perturbation theory.

4. One-loop perturbative analysis of the WI

A first indication of the cutoff effects related to a given choice of the topology $\mathcal{T}$ can be

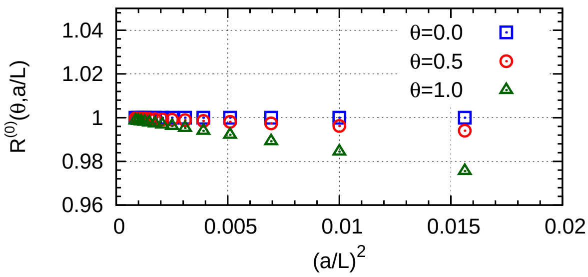

Figure 2: Continuum approach of $\mathcal{R}^{(0)}$ with topology $\mathcal{T} = 2$.

obtained in principle from a one-loop perturbative calculation of the WI. We anticipate that once the $\mathrm{O}(a)$-improvement has been carried out, the residual lattice artefacts of $\mathrm{O}(a^2)$ have comparable size in the various topologies, so that a conclusive argument for the choice of the preferred $\mathcal{T}$ has to follow from non-perturbative considerations. To show this, we expand the ratio $\mathcal{R}$ in powers of the coupling, i.e.

$$\mathcal{R} = \mathcal{R}^{(0)} + g_0^2 \mathcal{R}^{(1)} + \mathrm{O}(g_0^4) \ . \tag{4.1}$$

Each term of the perturbative expansion is a function of the bare quark mass m and must be computed at $m = m_{\rm cr}$. Since the latter depends in turn upon the bare coupling, each correlator h of eq. (3.13) has to be expanded according to

$$h = h^{(0)}|_{m=0} + g_0^2 \left[h^{(1)} + m_{\rm cr}^{(1)} \partial_m h^{(0)} + h_{\rm b}^{(1)} \right]_{m=0} + \mathrm{O}(g_0^4) \,, \tag{4.2}$$

where ∂_m indicates a partial derivative with respect to m and the subscript "b" denotes the contribution of the boundary counter-terms proportional to $\tilde{c}_{\rm t} - 1$. The one-loop critical mass $m_{\rm cr}^{(1)}$ is defined here by requesting that the $\mathrm{O}(a)$-improved PCAC quark mass vanish. Its values at finite lattice spacing are taken from [25, 26].

The ratio $\mathcal{R}$ is expected to be tree-level improved, since all the improvement counter-terms start at $\mathrm{O}(g_0^2)$. This expectation is confirmed by figure 2, where the approach of $\mathcal{R}^{(0)}$ to the continuum limit is reported for the topology $\mathcal{T} = 2$. We observe that the slope of $\mathcal{R}^{(0)}$ increases with θ (the scaling is perfect at $\theta = 0.0$) and is independent of $\mathcal{T}$. It follows that, in order to identify a better $\mathcal{T}$, at least the one-loop contribution has to be worked out explicitly.

The perturbative expansion of the two-point correlator $h_{\rm A}^{\rm I}$ has been discussed in [23] and will not be reviewed here. The one-loop coefficient of the three-point correlator $h_{\rm VA}^{\rm I(1)}$ receives contributions from Feynman diagrams corresponding to self-energy and tadpole corrections of the single quark legs, plus vertex corrections with gluons propagating from one leg to another.

Several possible improvement conditions may be imposed in order to tune $c_{\rm V}^{\rm stat(1)}$ so that the $\mathrm{O}(a)$-improvement is realized at one-loop order. After some attempts, we found that a reasonable definition is to enforce the equation

$$\mathcal{R}^{(1)}(\theta_1, a/L) = \mathcal{R}^{(1)}(\theta_2, a/L) + \mathrm{O}\left[(a/L)^2\right] \ , \tag{4.3}$$

	EH	APE
$c_{\rm V}^{\rm stat(1)}$	0.0048(3)	0.0185(3)

Table 2: $c_{\rm V}^{\rm stat(1)}$ for the EH and APE actions.

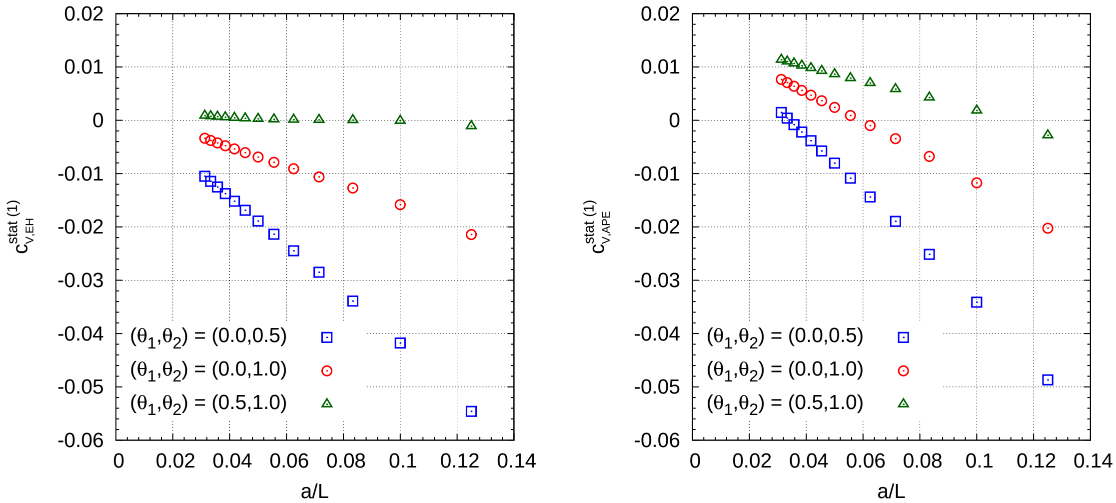

Figure 3: Continuum approach of $c_{\rm V}^{\rm stat(1)}$ for the EH (left plot) and APE (right plot) actions. Plots refer to the topology $\mathcal{T} = 2$. Different choices of the θ-angles provide independent definitions of $c_{\rm V}^{\rm stat(1)}$. Plotted points correspond to $L/a = 8, \ldots, 32$.

which defines $c_{\rm V}^{\rm stat(1)}$ up to O(a/L)-terms. Cutoff effects with the WI topology $\mathcal{T} = 2$ are reported in tables 6-7 and in figure 3 for the EH (left plot) and APE (right plot) actions and three possible choices of the pair (θ_1, θ_2). The other topologies show similar lattice artefacts. As expected, different definitions converge to the same continuum limit, which is very small for the EH discretization, if compared to the size of the cutoff effects, and somewhat larger for the APE action. It follows that the extrapolation of the lattice points to the continuum is difficult and one should not expect a high numerical precision. In order to reduce the size of the lattice artefacts, we have employed the blocking procedures of [27, 28]. Results are reported in table 2. Our determination of $c_{\rm V,EH}^{\rm stat(1)}$ is in good agreement with the original estimate given by [29] in the framework of NRQCD.

Once the improvement coefficient $c_{\rm V}^{\rm stat(1)}$ is known, the ratio $\mathcal{R}^{(1)}$ can be calculated in the O(a)-improved theory. In figure 4 its continuum approach is plotted vs. $(a/L)^2$ for all the topologies and the θ-angles. Corresponding data are reported in tables 8-9. The main feature of the plots is the similarity of the various definitions, which differ by just a few percent at the coarsest lattices. Nevertheless, some topologies are more sensitive to a change of θ than others, e.g. $\mathcal{T} = 4$ looks almost flat at $\theta = 1.0$, while it has the largest slope at $\theta = 0.0$. Remarkably, the spread between different $\mathcal{T}$'s almost vanishes around $\theta = 0.5$, thus suggesting that this θ-value could be the most stable against variations of the topology beyond perturbation theory.

We extract the common continuum limit of $\mathcal{R}^{(1)}$ via the afore-mentioned blocking tech-

JHEP01(2008)021

	EH	APE
$Z_{\rm A}^{\rm stat}/Z_{\rm V}^{\rm stat}$	$1-0.0521(1)g_0^2$	$1-0.0093(2)g_0^2$

Table 3: $Z_{\rm A}^{\rm stat}/Z_{\rm V}^{\rm stat}$ at one-loop order for the EH and APE actions.

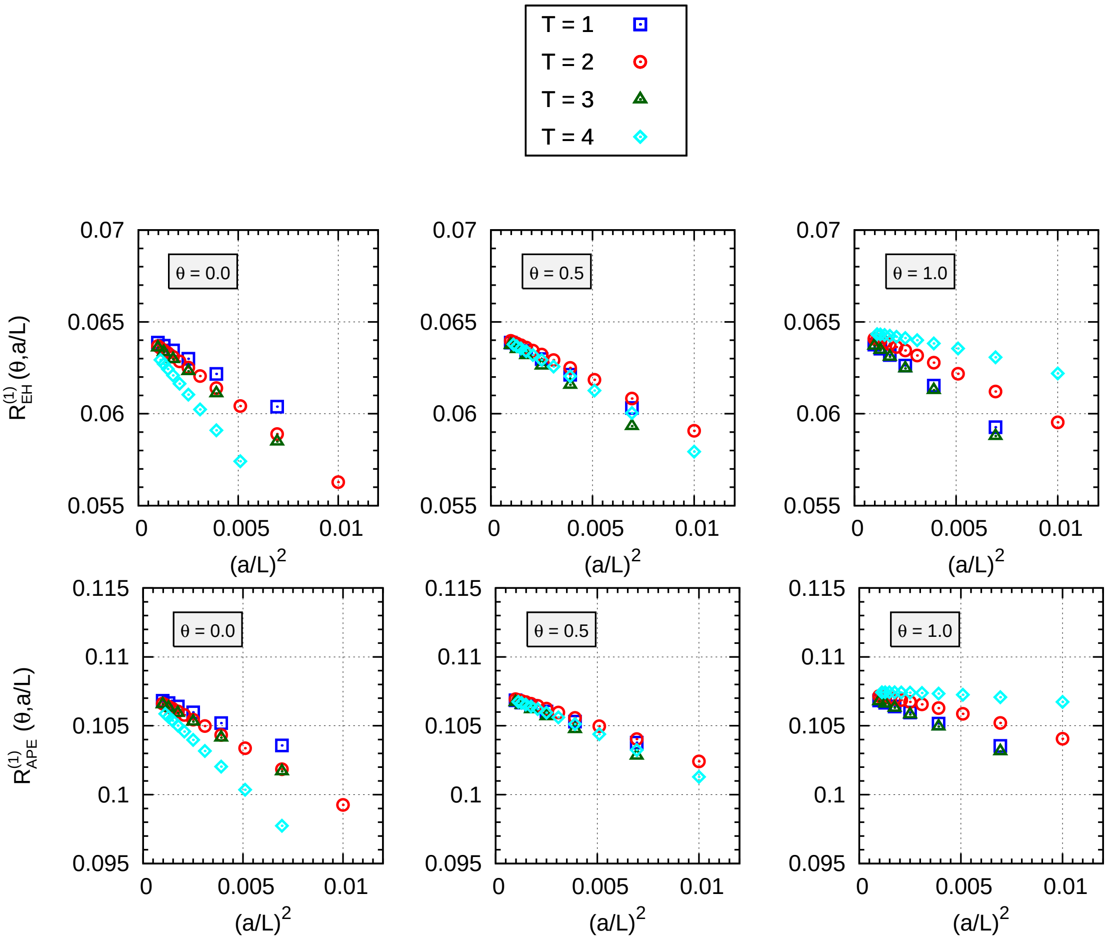

Figure 4: Continuum approach of $\mathcal{R}^{(1)}$ for the EH (upper plots) and APE (lower plots) actions. Plots refer to various SF topologies and θ angles. Plotted points correspond to $L/a = 10, \ldots, 32$ for $\mathcal{T} = 2, 4$ and $L/a = 12, \ldots, 32$ for $\mathcal{T} = 1, 3$.

niques. Our best estimates are $\mathcal{R}^{(1)}_{\rm EH} = 0.0644(1)$ and $\mathcal{R}^{(1)}_{\rm APE} = 0.1072(2)$. In order to isolate the ratio of the static renormalization constants $Z_{\rm A}^{\rm stat}/Z_{\rm V}^{\rm stat}$, the one-loop contribution of $Z_{\rm A}$, i.e. ${Z_{\rm A}}^{(1)} = -0.116458$ [30, 31], has to be subtracted from $\mathcal{R}^{(1)}$. Results are reported in table 3. The value obtained with the EH action is not novel: it checks the one previously found in [32, 14] within 3%.

5. Non-perturbative determination of $Z_{\rm A}^{\rm stat}/Z_{\rm V}^{\rm stat}$

In order to simulate the WI non-perturbatively, we first address the choice of the geo-

L/a	β	κ	θ
8	6.0219	0.135081,0.1344011	0.0,0.5,1.0
10	6.1628	0.135647,0.1351239	0.0,0.5,1.0
12	6.2885	0.135750,0.1353237	0.0,0.5,1.0
16	6.4956	0.135593,0.1352809	0.0,0.5,1.0

Table 4: Simulation parameters used for the non-perturbative study of the improvement coefficients $c_{\rm V}^{\rm stat}$, $b_{\rm V}^{\rm stat}$ and the ratio $Z_{\rm A}^{\rm stat}/Z_{\rm V}^{\rm stat}$.

metrical parameters. Some numerical attempts suggest that the topology with the best signal-to-noise ratio is also the one with the smallest aspect ratio T/L. This is largely expected on the basis of [6], since the loss of signal is mainly related to the temporal extension of the static propagator, which for every $\mathcal{T}$ goes from the boundary to $x_0 = T/2$. Given the lack of a clear indication from perturbation theory concerning the preeminence of a specific topology over the others, we decide to just follow the criterion of the signal-to-noise ratio and to consequently adopt $\mathcal{T} = 1$ for our non-perturbative study. Simulation parameters are collected in table 4. They have been taken from [6] and correspond to a physical size $L = 2L_{\rm max} = 1.436r_0$ of the SF. Moreover, $c_{\rm sw}$ is non-perturbatively tuned according to [24] and the boundary improvement coefficients $c_{\rm t}$ and $\tilde{c}_{\rm t}$ are respectively set to their two- and one-loop values [21].

It is worth noting that with $\mathcal{T} = 1$ the WI can be simulated directly at the chiral point, with no need for a mass extrapolation in the way of [33]. The κ-values which have been used are the ones reported on the left of the third column and correspond to $\kappa_{\rm cr}$ obtained from the O(a)-improved PCAC relation [11, 34].

We also observe that the simulation at $\beta = 6.1628$ cannot be actually performed with $t_1 = T/4$ and $t_2 = 3T/4$, since these are non-integer multiples of the lattice spacing in this particular case. To avoid the problem, we take here $t_1 = 2a$ and $t_2 = 7a$. This choice is theoretically sound since no contact term turns up in the WI. It amounts to changing the definition of $c_{\rm V}^{\rm stat}$ by an $\mathrm{O}(a)$-term and of the improved ratio $Z_{\rm A}^{\rm stat}/Z_{\rm V}^{\rm stat}$ by an $\mathrm{O}(a^2)$-term at that given β. Other choices are possible as well. The present one has the *a posteriori* advantage that it makes the β-dependence of $Z_{\rm A}^{\rm stat}/Z_{\rm V}^{\rm stat}$ smoother than other definitions.

To achieve a non-perturbative estimate of $Z_{\rm A}^{\rm stat}/Z_{\rm V}^{\rm stat}$ we first have to properly tune the improvement coefficient $c_{\rm V}^{\rm stat}$. We follow the perturbative definition introduced in eq. (4.3) and impose the improvement condition

$$\mathcal{R}(\theta_1, \beta) = \mathcal{R}(\theta_2, \beta) + \mathrm{O}(a^2)\,, \tag{5.1}$$

where, as already explained in section 3, the coefficients $c_{\rm A}^{\rm stat}$ and $c_{\rm A}$ are taken as input parameters. We stress once more that since $c_{\rm A}^{\rm stat}$ is known up to $\mathrm{O}(g_0^4)$-terms, this introduces a systematic uncertainty in our computation, thus making the numerical estimate of $c_{\rm V}^{\rm stat}$ only non-perturbatively effective. In principle, it could be possible to avoid this by enforcing two simultaneous conditions, i.e.

$$\begin{aligned}
&\mathcal{R}(\theta_1,\beta) = \mathcal{R}(\theta_2,\beta) + \mathrm{O}(a^2)\,, \\
&\mathcal{R}(\theta_1,\beta) = \mathcal{R}(\theta_3,\beta) + \mathrm{O}(a^2)\,, \qquad \theta_1 \neq \theta_2 \neq \theta_3\,,
\end{aligned} \tag{5.2}$$

from which $c_{\mathrm{A}}^{\mathrm{stat}}$ and $c_{\mathrm{V}}^{\mathrm{stat}}$ could be determined at the same time with no approximation. Unfortunately, the resulting expressions for the improvement coefficients are quite involved and characterized by a very poor signal. For this reason we are forced to resort to eq. (5.1). Being $\mathcal{R}$ linearly dependent on $c_{\mathrm{V}}^{\mathrm{stat}}$, i.e.

$$\mathcal{R}(\theta,\beta) = r(\theta,\beta) + c_{\mathrm{V}}^{\mathrm{stat}}(\beta)s(\theta,\beta)\,, \tag{5.3}$$

we obtain the improvement coefficient from the equation

$$c_{\mathrm{V}}^{\mathrm{stat}}(\beta) = -\frac{r(\theta_1,\beta) - r(\theta_2,\beta)}{s(\theta_1,\beta) - s(\theta_2,\beta)} \;+\; \mathrm{O}(a)\;. \tag{5.4}$$

Results at the simulation points are reported in table 12 of appendix A. Statistical errors have been computed through the jackknife method. In figure 5 the β-dependence of $c_{\mathrm{V}}^{\mathrm{stat}}$ is shown for different choices of the angles (θ_1,θ_2) and for different static discretizations. The most noticeable feature seems to be the large discrepancy with respect to the perturbative estimates given in the previous section. We also observe that the EH determination is quite distinct from the other regularizations, which are instead close to each other.

The numerical values of $c_{\mathrm{V}}^{\mathrm{stat}}$ should be independent of the choice of (θ_1,θ_2) up to $\mathrm{O}(a)$-effects. Therefore, the difference $\Delta c_{\mathrm{V}}^{\mathrm{stat}} = c_{\mathrm{V}}^{\mathrm{stat}}|_{(\theta_1,\theta_2)} - c_{\mathrm{V}}^{\mathrm{stat}}|_{(\theta_1',\theta_2')}$ is expected to decrease at larger β-values. This is confirmed by our data.

As table 12 shows, the improvement condition with the best signal-to-noise ratio is the one corresponding to $(\theta_1,\theta_2) = (0.5, 1.0)$. This is also the one with the smallest perturbative cutoff effects. A quadratic fit of it in the range of the Monte Carlo simulations $(6.0 \leq \beta \leq 6.5)$ leads to the parametrization

$$c_{\mathrm{V,EH}}^{\mathrm{stat}} = 0.694 - 0.732x + 0.330x^2\,, \tag{5.5}$$

$$c_{\mathrm{V,APE}}^{\mathrm{stat}} = 0.421 - 0.531x + 0.360x^2\,, \tag{5.6}$$

$$c_{\mathrm{V,HYP1}}^{\mathrm{stat}} = 0.453 - 0.584x + 0.421x^2\,, \tag{5.7}$$

$$c_{\mathrm{V,HYP2}}^{\mathrm{stat}} = 0.494 - 0.528x + 0.404x^2\,; \qquad x = \beta - 6\;. \tag{5.8}$$

The $\mathrm{O}(a)$-improved ratio of the renormalization constants $Z_{\mathrm{A}}^{\mathrm{stat}}/Z_{\mathrm{V}}^{\mathrm{stat}}$ corresponding to this choice of $c_{\mathrm{V}}^{\mathrm{stat}}$ is shown in figure 6; the same data are collected in table 13. To extract this ratio out of $\mathcal{R}$, we used the ALPHA determination of Z_{A} reported in [35]. Since now all the improvement counter-terms have been taken into account, the definition of $Z_{\mathrm{A}}^{\mathrm{stat}}/Z_{\mathrm{V}}^{\mathrm{stat}}$ with $\theta = 0.0$ has to agree up to $\mathrm{O}(a^2)$-terms with those at $\theta = 0.5$ and $\theta = 1.0$, which have been used in order to tune the improvement coefficient. Indeed, it can be seen from table 13 that the differences are zero within the statistical errors. Aside the non-perturbative determination, also the one-loop estimates of table 3 are reported in figure 6. The agreement is good with EH static fermions in the whole region explored

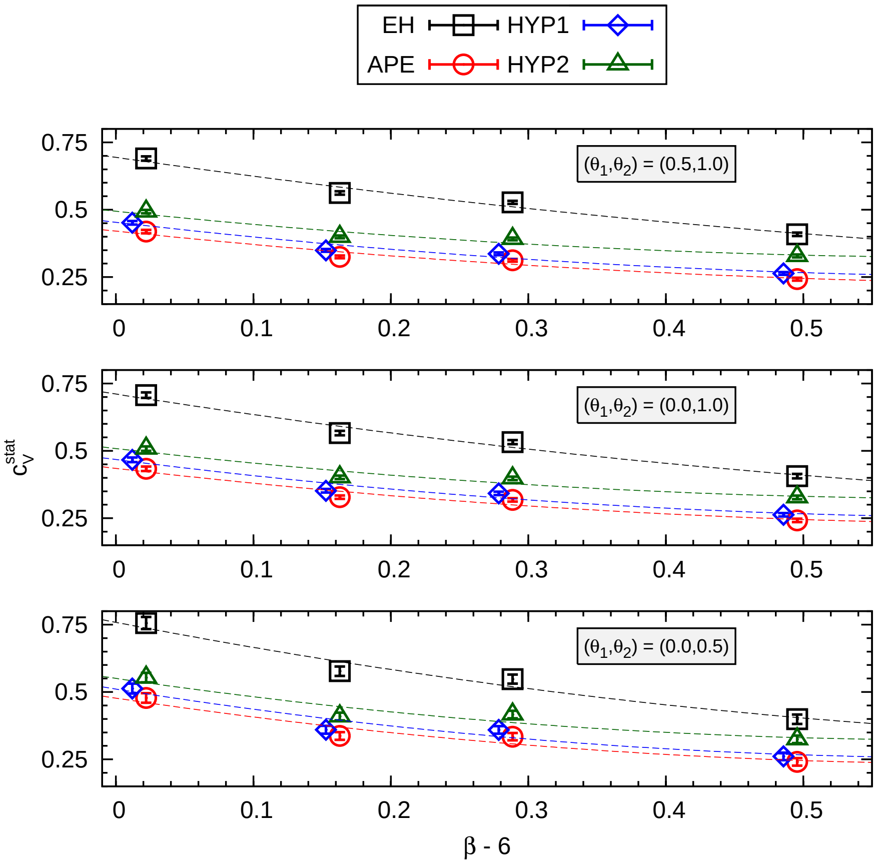

Figure 5: β-dependence of $c_{\rm V}^{\rm stat}$ for some choices of the pair (θ_1, θ_2) and of the static action. For the sake of readability, points (diamonds) have been slightly shifted along the horizontal axis. Dashed curves represent quadratic fits.

by the Monte Carlo simulations. It is good as well with the APE action at the largest β-values. A quadratic fit (in the range $6.0 \le \beta \le 6.5$) gives

$$\begin{aligned}
\left[Z_{\rm A}^{\rm stat}/Z_{\rm V}^{\rm stat}\right]_{\rm EH}(g_0) &= 0.953 + 0.0417x - 0.0828x^2\,, && (5.9)\\
\left[Z_{\rm A}^{\rm stat}/Z_{\rm V}^{\rm stat}\right]_{\rm APE}(g_0) &= 0.958 + 0.113x - 0.126x^2\,, && (5.10)\\
\left[Z_{\rm A}^{\rm stat}/Z_{\rm V}^{\rm stat}\right]_{\rm HYP1}(g_0) &= 0.963 + 0.109x - 0.131x^2\,, && (5.11)\\
\left[Z_{\rm A}^{\rm stat}/Z_{\rm V}^{\rm stat}\right]_{\rm HYP2}(g_0) &= 0.961 + 0.129x - 0.146x^2\;; \qquad x = \beta - 6\,. && (5.12)
\end{aligned}$$

Eqs. (5.9)–(5.12) reproduce the numbers of table 13 within the statistical errors. For convenience, we also report a parametrization of $Z_{\rm A}^{\rm stat}/Z_{\rm V}^{\rm stat}$ with all the improvement coefficients set to their respective values, but $c_{\rm A}^{\rm stat} = c_{\rm V}^{\rm stat} = 0$. With this choice, the WI is not O(a)-improved. Definitions corresponding to different choices of the θ-angle differ now

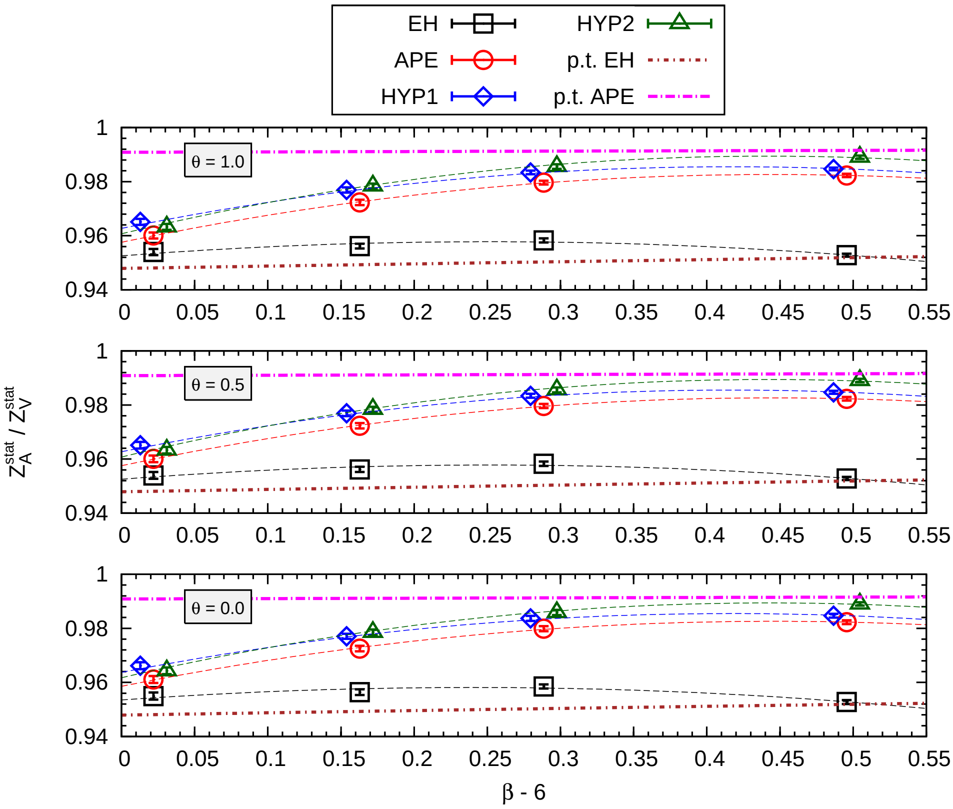

Figure 6: O(a)-improved ratio of the renormalization constants $Z_{\rm A}^{\rm stat}/Z_{\rm V}^{\rm stat}$ for various static actions. Different choices of θ correspond to independent definitions of the WI. For the sake of readability, points (diamonds and triangles) have been slightly shifted along the horizontal axis. Dashed curves represent quadratic fits.

by O(a)-terms, which are well above the statistical uncertainties. At $\theta = 0.5$ we find

$$\left[Z_{\rm A}^{\rm stat}/Z_{\rm V}^{\rm stat}\right]_{\rm EH}(g_0) \;=\; 0.818 + 0.186x - 0.134x^2\,, \tag{5.13}$$

$$\left[Z_{\rm A}^{\rm stat}/Z_{\rm V}^{\rm stat}\right]_{\rm APE}(g_0) \;=\; 0.917 + 0.176x - 0.165x^2\,, \tag{5.14}$$

$$\left[Z_{\rm A}^{\rm stat}/Z_{\rm V}^{\rm stat}\right]_{\rm HYP1}(g_0) \;=\; 0.926 + 0.178x - 0.177x^2\,, \tag{5.15}$$

$$\left[Z_{\rm A}^{\rm stat}/Z_{\rm V}^{\rm stat}\right]_{\rm HYP2}(g_0) \;=\; 0.978 + 0.158x - 0.179x^2\,; \qquad x = \beta - 6\,. \tag{5.16}$$

Our final results, represented by eqs. (5.9)–(5.12) depend upon the choice of $c_{\rm A}^{\rm stat}$. Adopting the determination of [6] introduces a systematic uncertainty at O(g_0^4), which propagates to the ratios $Z_{\rm A}^{\rm stat}/Z_{\rm V}^{\rm stat}$ and can be easily estimated. We first observe that the improvement coefficient $c_{\rm V}^{\rm stat}$ is very sensitive to variations of $c_{\rm A}^{\rm stat}$. This is not surprising, since both the counter-terms proportional to $c_{\rm V}^{\rm stat}$ and $c_{\rm A}^{\rm stat}$ are meant to cancel the O(a)-lattice artefacts of the WI. Therefore, a change of O(1) in $c_{\rm A}^{\rm stat}$ is expected to produce a variation of the same order in $c_{\rm V}^{\rm stat}$ via eq. (5.1). In practice, setting $c_{\rm A}^{\rm stat} = 0$ lowers the estimates of eqs. (5.5)–(5.8) by 30% at the coarsest lattice spacing. Nevertheless, if the new values of $c_{\rm V}^{\rm stat}|_{c_{\rm A}^{\rm stat}=0}$ are introduced in the WI and the counter-term of the static axial

JHEP01(2008)021

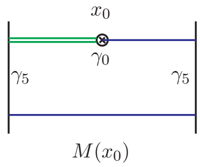

Figure 7: Three-point SF correlator.

current is explicitly dropped out at denominator of eq. (3.14), the variation of $Z_{\mathrm{A}}^{\mathrm{stat}}/Z_{\mathrm{V}}^{\mathrm{stat}}$ amounts to at most 1%. This is due to a very large numerical cancellation of $c_{\mathrm{A}}^{\mathrm{stat}}$ within the ratio $\mathcal{R}$. It follows that eqs. (5.9)–(5.12) can be assigned a systematic uncertainty of 1%.

Concerning the systematic uncertainty of $c_{\mathrm{V}}^{\mathrm{stat}}$, which has a strong dependence upon $c_{\mathrm{A}}^{\mathrm{stat}}$ in our determination, we naively expect that physical matrix elements of the static vector current will be only slightly affected by variations of $c_{\mathrm{V}}^{\mathrm{stat}}$, in strict analogy with the static axial current, where a change of the operator counter-term is compensated by an opposite variation in the renormalization constant, as shown in [36]. Unfortunately, we have no quantitative elements at the moment to clarify if this is the case also for the static vector current.

6. The improvement coefficient $b_{\mathrm{V}}^{\mathrm{stat}}$

The axial WI at non-zero light-quark mass is complicated by the presence of a mass term proportional to the temporal integral of the SF correlator $h_{\mathrm{VP}}^{\mathrm{I}}$ introduced in eq. (3.13). Since the integration region covers the whole interval $[t_1, t_2]$, an integrable contact term raises at $y_0 = x_0 = T/2$. Managing the integral can be disadvantageous in some cases: for instance, in perturbation theory it requires a complete one-loop calculation for each value of the integration variable, since no Fourier transform is defined in the SF along the time direction. Therefore, in order to improve the static vector current out of the chiral limit, it is easier to look for some more comfortable observable.

One attractive possibility is to consider a three-point SF correlator with the insertion of the static vector current in the bulk. To this aim we define

$$M^{\mathrm{I}}(x_0, m) = \langle \Sigma'^{21} V_0^{\mathrm{1h;I}}(x) \Sigma^{\mathrm{h2}} \rangle \,, \tag{6.1}$$

where Σ^{h2} has been introduced in eq. (3.4) and

$$\Sigma'^{21} = \frac{a^6}{L^3} \sum_{\mathbf{y}'\mathbf{z}'} \bar{\zeta}_2'(\mathbf{y}') \gamma_5 \zeta_1'(\mathbf{z}') \tag{6.2}$$

is a relativistic pseudoscalar boundary source localized at $x_0 = T$. Since we are interested in massive light-quarks, we keep the mass dependence explicit in the definition of M^{I}. The flavour structure of the chosen valence operators allows for just one Wick contraction, depicted in figure 7. To have it renormalized, all the logarithmic divergences must be

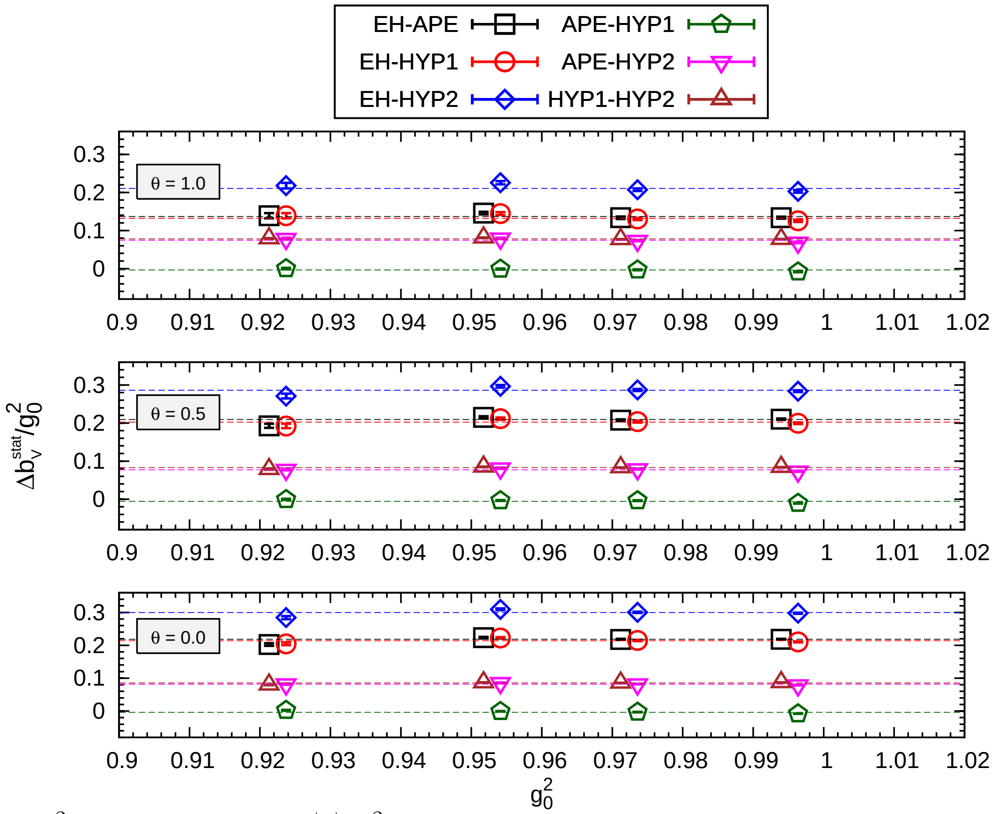

captiong_0^2-dependence of $\Delta b_{\rm V}^{\rm stat}/g_0^2$ corresponding to various combinations of the static actions and for some choices of the θ-angle. To improve the readability, points (squares and upper triangles) have been slightly shifted along the horizontal axis. Dashed lines represent fits to a constant.

subtracted, both those related to the static vector current and the ones induced by the boundary sources. In the O(a)-improved theory the renormalized correlator reads

$$M_{\rm R}^{\rm I}(x_0,m_{\rm R}) = Z_{\rm V}^{\rm stat} Z_\zeta^3 Z_\zeta^{\rm h}\{1+b_\zeta a m_{\rm q}\}^3\{1+b_{\rm V}^{\rm stat} a m_{\rm q}\} M^{\rm I}(x_0,m)\ . \tag{6.3}$$

In order to get rid of the renormalization constants, we construct the ratio of $M_{\rm R}^{\rm I}$ at two different values of the renormalized light-quark mass, i.e. $Lm_{\rm R}=0.24$ and $Lm_{\rm R}=0$. This is not sufficient to isolate $b_{\rm V}^{\rm stat}$, since the improvement of the boundary light-quark source contains b_ζ, which does not drop out in the ratio. Nevertheless, b_ζ is independent of the static action. Therefore, it cancels when we enforce the improvement condition that the ratio of the three-point SF correlator be the same with two different static actions $\rm S_1$ and $\rm S_2$ up to O(a^2)-terms, i.e.

$$\{1+b_{\rm V,S_1}^{\rm stat} a m_{\rm q}\}\frac{M^{\rm I}(T/2,m)}{M^{\rm I}(T/2,m_{\rm cr})}\bigg|_{\rm S_1} = \{1+b_{\rm V,S_2}^{\rm stat} a m_{\rm q}\}\frac{M^{\rm I}(T/2,m)}{M^{\rm I}(T/2,m_{\rm cr})}\bigg|_{\rm S_2} + {\rm O}(a^2)\ . \tag{6.4}$$

In the above equation, we decided to place the operator insertion in the middle of the bulk and to choose $T/L=1$. This improvement condition provides a non-perturbative definition of $\Delta b_{\rm V}^{\rm stat} = b_{\rm V,S_1}^{\rm stat} - b_{\rm V,S_2}^{\rm stat}$.

Simulations have been performed according to the parameters reported in table 4. In particular, the κ-values on the right of the third column correspond to $Lm_{\rm R} = 0.24$, with $m_{\rm R}$ the quark mass renormalized in the SF scheme at scale $\mu = 1/(1.436r_0)$. Numerical results of $\Delta b_{\rm V}^{\rm stat}$ are reported in table 14 for the various independent combinations of the static actions and the usual θ-angles. They are also represented in figure 6, where $\Delta b_{\rm V}^{\rm stat}/g_0^2$ is plotted vs. g_0^2. A remarkable feature of the results is their flatness in g_0^2. Since

$$b_{\rm V}^{\rm stat} = \frac{1}{2} + b_{\rm V}^{\rm stat(1)} g_0^2 + O(g_0^4)\,, \tag{6.5}$$

this could be interpreted as a good signal of scaling and could lead to the prompt conclusion that $\Delta b_{\rm V}^{\rm stat}$ is not dominated by $\mathrm{O}(g_0^4)$-terms. Nevertheless, we observe that g_0^2 varies from 0.924 to 0.996 in the range of the simulations, i.e. it changes by only 8%. Such a small variation could be well compatible with a slight change of the differences $\Delta b_{\rm V}^{\rm stat}$ even in a region not strictly close to the scaling one.

A second observation is that all the differences involving the EH action have a significant dependence on θ, with spreads varying from 30% to 60% at the various bare gauge couplings. This is a clear indication that large non-perturbative $\mathrm{O}(a)$ lattice artefacts affect our definition of $b_{\rm V,EH}^{\rm stat}$ based on the three-point SF correlator $M^{\rm I}$. On the contrary, the remaining differences, involving exclusively the ALPHA actions, are much more universal in θ: in these cases the spread among different definitions stays always below 0.01.

A fit of $\Delta b_{\rm V}^{\rm stat}/g_0^2$ to a constant provides an effective non-perturbative parametrization of the difference of the improvement coefficients in the region of the Monte Carlo simulations. Since we have no theoretical argument to privilege one particular definition over the others, we decide to average the results of the fits corresponding to the three θ-values and to assign the averages an absolute uncertainty as large as the maximal discrepancy between different θ-determinations. In this way we obtain

$$(\Delta b_{\rm V}^{\rm stat})_{\rm EH-APE} = 0.19(8) g_0^2\,, \tag{6.6}$$
$$(\Delta b_{\rm V}^{\rm stat})_{\rm EH-HYP1} = 0.18(8) g_0^2\,, \tag{6.7}$$
$$(\Delta b_{\rm V}^{\rm stat})_{\rm EH-HYP2} = 0.27(9) g_0^2\,, \tag{6.8}$$
$$(\Delta b_{\rm V}^{\rm stat})_{\rm APE-HYP1} = -0.004(2) g_0^2\,, \tag{6.9}$$
$$(\Delta b_{\rm V}^{\rm stat})_{\rm APE-HYP2} = 0.078(7) g_0^2\,, \tag{6.10}$$
$$(\Delta b_{\rm V}^{\rm stat})_{\rm HYP1-HYP2} = 0.082(7) g_0^2\,. \tag{6.11}$$

In order to isolate the improvement coefficient $b_{\rm V}^{\rm stat}$ corresponding to each static action, we perform an analytical one-loop perturbative calculation of $b_{\rm V,EH}^{\rm stat}$ and $b_{\rm V,APE}^{\rm stat}$. To this aim, we expand the three-point SF correlator in powers of g_0^2, i.e.

$$\begin{aligned} M^{\rm I}(x_0,m) = {} & M^{(0)}(x_0,m^{(0)}) + \\ & + g_0^2 \left[M^{\rm I(1)}\left(x_0,m^{(0)}\right) + m^{(1)}\partial_m M^{(0)}\left(x_0,m^{(0)}\right) + M_{\rm b}^{\rm I(1)}\left(x_0,m^{(0)}\right)\right] + \\ & + \mathrm{O}(g_0^4)\,, \end{aligned} \tag{6.12}$$

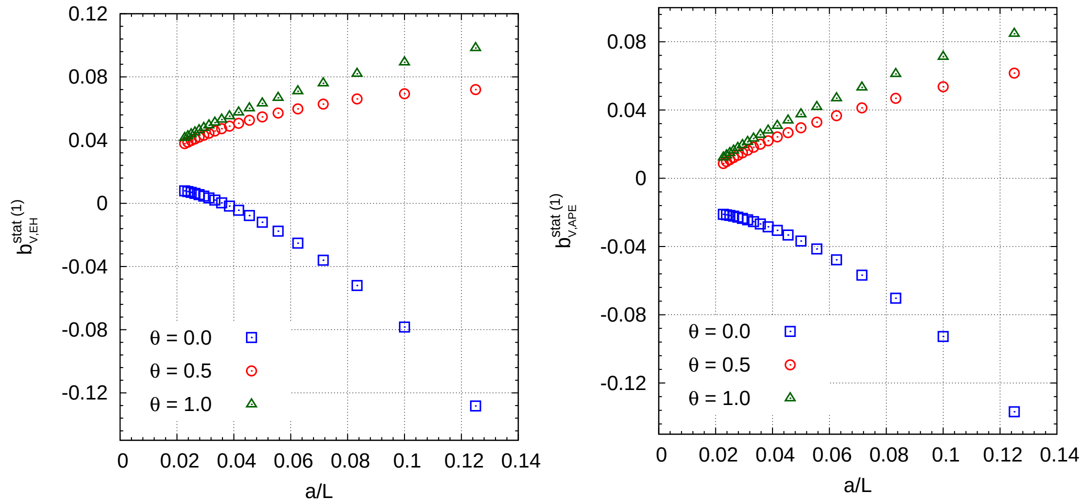

Figure 8: Continuum approach of $b_{\rm V}^{\rm stat(1)}$ for the EH (left plot) and APE (right plot) actions. Different choices of the θ-angle provide independent definitions of $b_{\rm V}^{\rm stat(1)}$. Plotted points correspond to $L/a = 8, \ldots, 46$.

	EH	APE
$b_{\rm V}^{\rm stat(1)}$	0.013(1)	-0.018(1)

Table 5: $b_{\rm V}^{\rm stat(1)}$ for the EH and APE actions.

where the perturbative coefficients of the bare quark mass $m^{(0)}$ and $m^{(1)}$ are chosen according to eqs. (3.29)-(3.30) of [37]. Here $m_{\rm R}$ is defined as the renormalized quark mass in the minimal subtraction scheme on the lattice at scale $\mu = 1/L$. In this perturbative calculation we impose the improvement condition

$$\frac{M_{\rm R}^{\rm I}(T/2, 0.24/L)}{M_{\rm R}^{\rm I}(T/2, 0)} = \text{const.} + {\rm O}(a^2)\,, \tag{6.13}$$

with aspect ratio $T/L = 1$ and $\theta = 0.0, 0.5, 1.0$. When expanded in perturbation theory, this equation provides for a definition of $b_{\rm V}^{\rm stat(1)} + 3b_\zeta^{(1)}$ up to O(a/L)-terms. Since $b_\zeta^{(1)} = -0.06738(4) \times C_{\rm F}$ has been previously calculated in [37], this is sufficient to isolate $b_{\rm V}^{\rm stat(1)}$. Lattice data are reported in tables 10–11 and plotted in figure 8. Their continuum extrapolation leads to the estimates quoted in table 5. These correspond in turn to an exact one-loop difference

$$(\Delta b_{\rm V}^{\rm stat})^{(1)}_{\rm EH-APE} = 0.0324(4)\,, \tag{6.14}$$

which is quite a bit off the central value of eq. (6.6). Clearly, this difference may be attributed to the presence of non-negligible O(g_0^4)-terms, which in principle could be there. However, the systematic uncertainty which characterizes the definition of the improvement coefficient with the EH action prevents us from making a more precise statement. For this reason, we desist from quoting a final estimate of $b_{\rm V,EH}^{\rm stat}$. Instead, we use $b_{\rm V,APE}^{\rm stat(1)}$ to solve

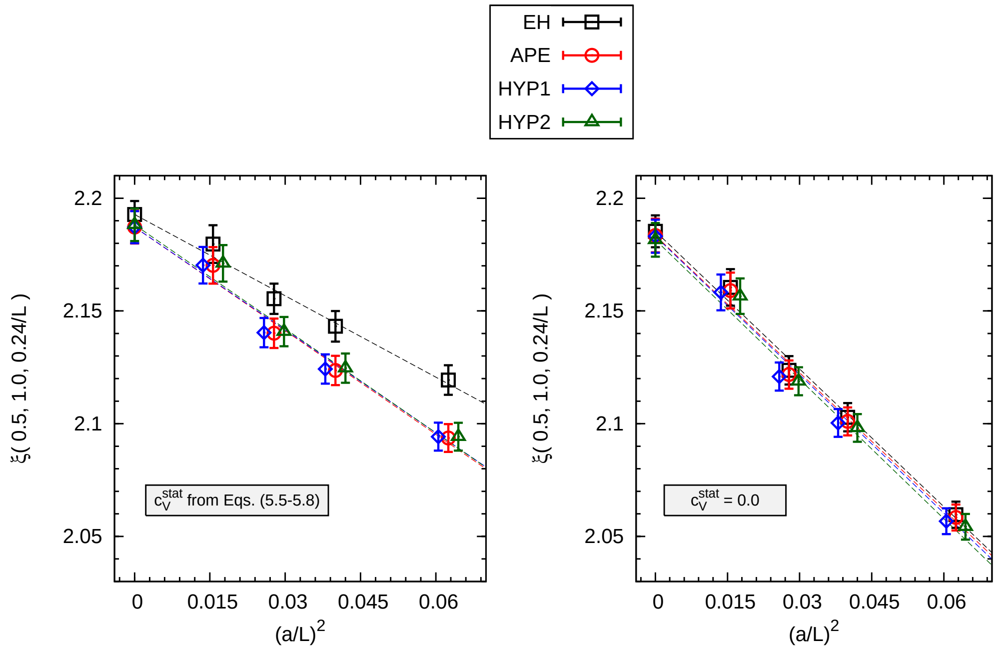

Figure 9: Scaling plots for $\xi(0.5, 1.0, 0.24/L)$. To improve the readability, some of the points (diamonds and triangles) have been slightly shifted along the horizontal axis. Dashed curves represent independent linear fits in $(a/L)^2$. Continuum extrapolated values are also shown.

eqs. (6.9)–(6.10) and quote

$$b^{\mathrm{stat}}_{\mathrm{V,HYP1}} \approx \frac{1}{2} - 0.014(3)g_0^2 + \mathrm{O}(g_0^4)\,, \tag{6.15}$$

$$b^{\mathrm{stat}}_{\mathrm{V,HYP2}} \approx \frac{1}{2} - 0.096(8)g_0^2 + \mathrm{O}(g_0^4)\;. \tag{6.16}$$

The reader should not be surprised to see that the difference $(\Delta b^{\mathrm{stat}}_{\mathrm{V}})^{(1)}_{\mathrm{EH-APE}}$ given in eq. (6.14) is more precise than the single values of $b^{\mathrm{stat}}_{\mathrm{V}}$ reported in table 5. Indeed, the continuum estimate of eq. (6.14) has been obtained by extrapolating the difference of the lattice data reported in tables 10–11. Part of the cutoff effects drops out in this difference, which makes the continuum extrapolation easier.

6.1 A scaling test for $c^{\mathrm{stat}}_{\mathrm{V}}$

Our non-perturbative data enable a scaling test of the three-point SF correlator M^{I}, useful to assess the effectiveness of our numerical determination of $c^{\mathrm{stat}}_{\mathrm{V}}$. To this aim we introduce the ratio

$$\xi(\theta_1, \theta_2, m_{\mathrm{R}}) = \frac{M^{\mathrm{I}}(T/2, m_{\mathrm{R}})|_{\theta_1}}{M^{\mathrm{I}}(T/2, m_{\mathrm{R}})|_{\theta_2}}\,, \tag{6.17}$$

which has a well defined continuum limit, with a theoretical rate of convergence proportional to $\mathrm{O}(a^2)$ if the light-quark action is $\mathrm{O}(a)$-improved and $c^{\mathrm{stat}}_{\mathrm{V}}$ is properly tuned.

Figure 9 illustrates the approach of ξ to the continuum, corresponding to the choice of parameters $\theta_1 = 0.5$, $\theta_2 = 1.0$ and $Lm_{\rm R} = 0.24$. The left plot refers to the non-perturbative choice of $c_{\rm V}^{\rm stat}$ provided by eqs. (5.5)–(5.8); the right plot shows the unimproved case with $c_{\rm V}^{\rm stat} = 0$. Similar plots are obtained with different θ-angles and $m_{\rm R}$.

We observe that all the static actions give comparable results and statistical uncertainties at finite lattice spacing, save for the EH one in the improved case. If we look at the right plot, we note that the total variation of ξ in the simulation region is only about 5%. This can be attributed to a significant cancellation of the $\mathrm{O}(a)$ lattice artefacts between numerator and denominator, which on one hand gives ξ a good scaling behaviour also in absence of operator improvement, but on the other makes it rather insensitive to a change of $c_{\rm V}^{\rm stat}$. Nevertheless, we find that once $c_{\rm V}^{\rm stat}$ is switched on, the total variation of ξ in the simulation region drops to 3%, corresponding to a flatter approach to the continuum. As it might be expected, the strongest effect of $c_{\rm V}^{\rm stat}$ is at $L/a = 8$, where the central values of the lattice points are shifted by 1.5-2.9%.

7. Conclusions

In this paper we have studied the renormalization of the static vector current and its $\mathrm{O}(a)$-improvement in the quenched approximation of lattice QCD. Quark degrees of freedom are described by lattice Wilson-type fermions in the light sector and various discretizations of the static fermions, including those introduced some years ago by the ALPHA Collaboration (APE, HYP1, HYP2).

Owing to the chiral symmetry of the continuum theory, the RG running of the static vector and axial currents coincides. Since the latter has been extensively studied in the literature, a complete description of the renormalization factor $Z_{\rm V}^{\rm stat}$ is achieved by simply fixing the ratio of the two renormalized currents at a given reference scale (in our study $\mu_{\rm ref}^{-1} = 2L_{\rm max} = 1.436 r_0$). To this aim we make use of an appropriate axial Ward identity in the framework of the Schrödinger functional. The enforcement of chiral symmetry up to $\mathrm{O}(a^2)$-terms provides us with a lever to tune the improvement coefficient $c_{\rm V}^{\rm stat}$. Unfortunately, the resulting determination is not fully non-perturbative, since it relies upon a previous computation of $c_{\rm A}^{\rm stat}$ which is only effective, i.e. correct up to $\mathrm{O}(g_0^4)$-terms. With regard to the numerical results, a comparison of the Monte Carlo simulations with a one-loop perturbative calculation shows that large higher-order contributions affect $c_{\rm V}^{\rm stat}$ within the explored region of the gauge coupling ($6.0 \le \beta \le 6.5$). On the other hand, we observe a good agreement between the non-perturbative determination of the $\mathrm{O}(a)$-improved ratio $Z_{\rm A}^{\rm stat}/Z_{\rm V}^{\rm stat}$ and its one-loop approximation.

The $\mathcal{O}(a)$-improvement programme is carried out at non-zero light-quark mass via the introduction of a second improvement coefficient $b_{\rm V}^{\rm stat}$. This is tuned on the basis of an independent condition involving a boundary-to-boundary three-point correlator of the static vector current, out of the chiral limit. The coefficient $b_{\rm V}^{\rm stat}$ is studied at one-loop order in perturbation theory for the EH and APE actions. To extend our study to the HYP actions, where perturbation theory is not easily handled, we adopt a mixed strategy: the difference $\Delta b_{\rm V}^{\rm stat}$ of the improvement coefficients between two different static discretizations is computed non-perturbatively and the one-loop estimate with the APE action is used to isolate $b_{\rm V}^{\rm stat}$ in the HYP1 and HYP2 cases up to $\mathrm{O}(g_0^4)$-terms. It has to be said that a direct comparison of the non-perturbative estimate of $(\Delta b_{\rm V}^{\rm stat})_{\rm EH-APE}$ with its one-loop value shows that the amount of such $\mathrm{O}(g_0^4)$-terms could be non-negligible and hard to control. Nevertheless, this problem seems to characterize the EH fermions more than their statistically improved versions, for which a better agreement with perturbation theory is expected on the basis of the experience gathered by the ALPHA Collaboration in previous studies of the static axial current.

Anyway, one should always keep in mind that $b_{\rm V}^{\rm stat}$ enters the improved static vector current accompanied by a factor of $am_{\rm q}$, which is rather small at light-quark masses up to the strange one and the commonly affordable lattice spacings. In this sense, it constitutes a subdominant contribution, which is not expected to have a crucial effect on the scaling behaviour of phenomenological matrix elements of the static vector current with external B_d- or B_s-meson states.

Acknowledgments

A special thanks goes to R. Sommer for invaluable support during all the stages of this work. We also thank D. Guazzini, M. Della Morte, M. Papinutto, C. Pena and H. Wittig for useful discussions. Partial financial support from the Alexander-von-Humboldt Stiftung is acknowledged. We acknowledge DESY Hamburg and the Institut für Kernphysik - Universität Mainz for providing hospitality during the intermediate stage of the project, as well as the computing centre of DESY Zeuthen for its technical support. This work was supported in part by the EU Contract No. MRTN-CT-2006-035482, “FLAVIAnet”.

JHEP01(2008)021

A. Additional tables

L/a	$c^{\mathrm{stat}(1)}_{\mathrm{V,EH}}\big\|_{(\theta_1,\theta_2)=(0.0,0.5)}$	$c^{\mathrm{stat}(1)}_{\mathrm{V,EH}}\big\|_{(\theta_1,\theta_2)=(0.0,1.0)}$	$c^{\mathrm{stat}(1)}_{\mathrm{V,EH}}\big\|_{(\theta_1,\theta_2)=(0.5,1.0)}$
4	$-1.21318905506 \times 10^{-1}$	$-5.56860354782 \times 10^{-2}$	$-1.14115660920 \times 10^{-2}$
6	$-8.05799533807 \times 10^{-2}$	$-3.56181870915 \times 10^{-2}$	$-7.37458670533 \times 10^{-3}$
8	$-5.45943895816 \times 10^{-2}$	$-2.14296960443 \times 10^{-2}$	$-1.11423236142 \times 10^{-3}$
10	$-4.17792968218 \times 10^{-2}$	$-1.58212044566 \times 10^{-2}$	$-1.04666543337 \times 10^{-4}$
12	$-3.39132673910 \times 10^{-2}$	$-1.27133821723 \times 10^{-2}$	$4.11644560339 \times 10^{-5}$
14	$-2.84872496446 \times 10^{-2}$	$-1.06310641447 \times 10^{-2}$	$7.08421808901 \times 10^{-5}$
16	$-2.44775851326 \times 10^{-2}$	$-9.08817318086 \times 10^{-3}$	$1.12471960839 \times 10^{-4}$
18	$-2.13776226148 \times 10^{-2}$	$-7.87813705828 \times 10^{-3}$	$1.78912840345 \times 10^{-4}$
20	$-1.89020434292 \times 10^{-2}$	$-6.89431955817 \times 10^{-3}$	$2.63691059080 \times 10^{-4}$
22	$-1.68756672083 \times 10^{-2}$	$-6.07394710919 \times 10^{-3}$	$3.59366131023 \times 10^{-4}$
24	$-1.51841738803 \times 10^{-2}$	$-5.37672581715 \times 10^{-3}$	$4.60431552309 \times 10^{-4}$
26	$-1.37494665187 \times 10^{-2}$	$-4.77520683457 \times 10^{-3}$	$5.63221867541 \times 10^{-4}$
28	$-1.25162477343 \times 10^{-2}$	$-4.24986678175 \times 10^{-3}$	$6.65402844941 \times 10^{-4}$
30	$-1.14441713189 \times 10^{-2}$	$-3.78634326450 \times 10^{-3}$	$7.65528806751 \times 10^{-4}$
32	$-1.05031230408 \times 10^{-2}$	$-3.37380171813 \times 10^{-3}$	$8.62744511694 \times 10^{-4}$

Table 6: Three different determinations of the one-loop contribution to $c_{\mathrm{V}}^{\mathrm{stat}}$ with EH static fermions according to the improvement condition eq. (4.3). Numbers refer to the topology $\mathcal{T} = 2$.

L/a	$c^{\mathrm{stat}(1)}_{\mathrm{V,APE}}\big\|_{(\theta_1,\theta_2)=(0.0,0.5)}$	$c^{\mathrm{stat}(1)}_{\mathrm{V,APE}}\big\|_{(\theta_1,\theta_2)=(0.0,1.0)}$	$c^{\mathrm{stat}(1)}_{\mathrm{V,APE}}\big\|_{(\theta_1,\theta_2)=(0.5,1.0)}$
4	$-1.22686673290 \times 10^{-1}$	$-6.58409712344 \times 10^{-2}$	$-2.74941292579 \times 10^{-2}$
6	$-7.75983902179 \times 10^{-2}$	$-3.92522157408 \times 10^{-2}$	$-1.51643269042 \times 10^{-2}$
8	$-4.86871345865 \times 10^{-2}$	$-2.02408469320 \times 10^{-2}$	$-2.81570404300 \times 10^{-3}$
10	$-3.41205392729 \times 10^{-2}$	$-1.17290094210 \times 10^{-2}$	$1.82812424278 \times 10^{-3}$
12	$-2.51362502419 \times 10^{-2}$	$-6.77983138946 \times 10^{-3}$	$4.26399256380 \times 10^{-3}$
14	$-1.89433155853 \times 10^{-2}$	$-3.44517803597 \times 10^{-3}$	$5.84345845792 \times 10^{-3}$
16	$-1.43758718224 \times 10^{-2}$	$-9.98819307355 \times 10^{-4}$	$6.99872560335 \times 10^{-3}$
18	$-1.08514987939 \times 10^{-2}$	$8.93569798294 \times 10^{-4}$	$7.90351127450 \times 10^{-3}$
20	$-8.04166342915 \times 10^{-3}$	$2.41124455308 \times 10^{-3}$	$8.64240269108 \times 10^{-3}$
22	$-5.74490428783 \times 10^{-3}$	$3.66095340524 \times 10^{-3}$	$9.26291571099 \times 10^{-3}$
24	$-3.83000893356 \times 10^{-3}$	$4.71111391836 \times 10^{-3}$	$9.79458495765 \times 10^{-3}$
26	$-2.20751253184 \times 10^{-3}$	$5.60799879909 \times 10^{-3}$	$1.02571343800 \times 10^{-2}$
28	$-8.14172229101 \times 10^{-4}$	$6.38421491915 \times 10^{-3}$	$1.06644451570 \times 10^{-2}$
30	$3.96087085934 \times 10^{-4}$	$7.06350798921 \times 10^{-3}$	$1.10266744094 \times 10^{-2}$
32	$1.45762004875 \times 10^{-3}$	$7.66362155507 \times 10^{-3}$	$1.13514918436 \times 10^{-2}$

Table 7: Three different determinations of the one-loop contribution to $c_{\mathrm{V}}^{\mathrm{stat}}$ with APE static fermions according to the improvement condition eq. (4.3). Numbers refer to the topology $\mathcal{T} = 2$.

L/a	$\mathcal{R}^{(1)}_{\rm EH}(\theta=0.0)$	$\mathcal{R}^{(1)}_{\rm EH}(\theta=0.5)$	$\mathcal{R}^{(1)}_{\rm EH}(\theta=1.0)$
4	$3.30112791641 \times 10^{-2}$	$5.07890218387 \times 10^{-2}$	$5.32679355672 \times 10^{-2}$
6	$3.95982301495 \times 10^{-2}$	$4.76144903008 \times 10^{-2}$	$4.87823906356 \times 10^{-2}$
8	$5.12452416492 \times 10^{-2}$	$5.53446719297 \times 10^{-2}$	$5.54812561435 \times 10^{-2}$
10	$5.62747608283 \times 10^{-2}$	$5.87919096424 \times 10^{-2}$	$5.88023249365 \times 10^{-2}$
12	$5.88913680345 \times 10^{-2}$	$6.05967926872 \times 10^{-2}$	$6.05933519321 \times 10^{-2}$
14	$6.04217811204 \times 10^{-2}$	$6.16508787417 \times 10^{-2}$	$6.16457789162 \times 10^{-2}$
16	$6.13931315301 \times 10^{-2}$	$6.23177973609 \times 10^{-2}$	$6.23106907219 \times 10^{-2}$
18	$6.20478428063 \times 10^{-2}$	$6.27659838840 \times 10^{-2}$	$6.27559138013 \times 10^{-2}$
20	$6.25099352992 \times 10^{-2}$	$6.30815917333 \times 10^{-2}$	$6.30682137670 \times 10^{-2}$
22	$6.28481782065 \times 10^{-2}$	$6.33122587177 \times 10^{-2}$	$6.32956656095 \times 10^{-2}$
24	$6.31031850685 \times 10^{-2}$	$6.34860186764 \times 10^{-2}$	$6.34665140076 \times 10^{-2}$
26	$6.33001903502 \times 10^{-2}$	$6.36202279760 \times 10^{-2}$	$6.35981895849 \times 10^{-2}$
28	$6.34555419363 \times 10^{-2}$	$6.37260940915 \times 10^{-2}$	$6.37019044423 \times 10^{-2}$
30	$6.35802087156 \times 10^{-2}$	$6.38111147867 \times 10^{-2}$	$6.37851294648 \times 10^{-2}$
32	$6.36817718015 \times 10^{-2}$	$6.38804596546 \times 10^{-2}$	$6.38529951792 \times 10^{-2}$

Table 8: Three different determinations of the one-loop contribution to the O(a)-improved WI with EH static fermions. Numbers refer to the topology $\mathcal{T}=2$.

L/a	$\mathcal{R}^{(1)}_{\rm APE}(\theta=0.0)$	$\mathcal{R}^{(1)}_{\rm APE}(\theta=0.5)$	$\mathcal{R}^{(1)}_{\rm APE}(\theta=1.0)$
4	$7.83613664415 \times 10^{-2}$	$9.63395380897 \times 10^{-2}$	$1.02312037738 \times 10^{-1}$
6	$8.29999758507 \times 10^{-2}$	$9.07196239420 \times 10^{-2}$	$9.31211717407 \times 10^{-2}$
8	$9.43090648772 \times 10^{-2}$	$9.79649261355 \times 10^{-2}$	$9.83100792082 \times 10^{-1}$
10	$9.92568717719 \times 10^{-2}$	$1.01312590309 \times 10^{-1}$	$1.01130674952 \times 10^{-1}$
12	$1.01847718258 \times 10^{-1}$	$1.03111765757 \times 10^{-1}$	$1.02755357444 \times 10^{-1}$
14	$1.03368358402 \times 10^{-1}$	$1.04185677884 \times 10^{-1}$	$1.03765015807 \times 10^{-1}$
16	$1.04335470132 \times 10^{-1}$	$1.04878533404 \times 10^{-1}$	$1.04436312823 \times 10^{-1}$
18	$1.04988139034 \times 10^{-1}$	$1.05352674754 \times 10^{-1}$	$1.04907826792 \times 10^{-1}$
20	$1.05449158322 \times 10^{-1}$	$1.05692363172 \times 10^{-1}$	$1.05253903968 \times 10^{-1}$
22	$1.05786795092 \times 10^{-1}$	$1.05944779845 \times 10^{-1}$	$1.05517080769 \times 10^{-1}$
24	$1.06041438462 \times 10^{-1}$	$1.06138003224 \times 10^{-1}$	$1.05723087837 \times 10^{-1}$
26	$1.06238214652 \times 10^{-1}$	$1.06289597523 \times 10^{-1}$	$1.05888244607 \times 10^{-1}$
28	$1.06393415756 \times 10^{-1}$	$1.06411014965 \times 10^{-1}$	$1.06023326229 \times 10^{-1}$
30	$1.06517980204 \times 10^{-1}$	$1.06509988458 \times 10^{-1}$	$1.06135695966 \times 10^{-1}$
32	$1.06619471630 \times 10^{-1}$	$1.06591897793 \times 10^{-1}$	$1.06230536156 \times 10^{-1}$

Table 9: Three different determinations of the one-loop contribution to the O(a)-improved WI with APE static fermions. Numbers refer to the topology $\mathcal{T}=2$.

JHEP01(2008)021

L/a	$b^{\mathrm{stat}(1)}_{\mathrm{V,EH}}(\theta=0.0)$	$b^{\mathrm{stat}(1)}_{\mathrm{V,EH}}(\theta=0.5)$	$b^{\mathrm{stat}(1)}_{\mathrm{V,EH}}(\theta=1.0)$
6	$-1.92494990552 \times 10^{-1}$	$7.59451390152 \times 10^{-2}$	$7.94433253811 \times 10^{-2}$
8	$-1.28284962759 \times 10^{-1}$	$7.19668221779 \times 10^{-2}$	$9.82580984223 \times 10^{-2}$
10	$-7.83097066265 \times 10^{-2}$	$6.93670764950 \times 10^{-2}$	$8.92282752595 \times 10^{-2}$
12	$-5.20449399705 \times 10^{-2}$	$6.60882882658 \times 10^{-2}$	$8.20217785512 \times 10^{-2}$
14	$-3.59939921230 \times 10^{-2}$	$6.27858498787 \times 10^{-2}$	$7.59502707254 \times 10^{-2}$
16	$-2.52419762755 \times 10^{-2}$	$5.97829596381 \times 10^{-2}$	$7.09345102910 \times 10^{-2}$
18	$-1.76143672046 \times 10^{-2}$	$5.71059870738 \times 10^{-2}$	$6.67548992369 \times 10^{-2}$
20	$-1.19885067448 \times 10^{-2}$	$5.47150817151 \times 10^{-2}$	$6.32117968093 \times 10^{-2}$
22	$-7.71840193796 \times 10^{-3}$	$5.25663880980 \times 10^{-2}$	$6.01574097982 \times 10^{-2}$
24	$-4.40467430491 \times 10^{-3}$	$5.06225291197 \times 10^{-2}$	$5.74858429769 \times 10^{-2}$
26	$-1.78765598057 \times 10^{-3}$	$4.88528309736 \times 10^{-2}$	$5.51202560392 \times 10^{-2}$
28	$3.08255934246 \times 10^{-4}$	$4.72321849465 \times 10^{-2}$	$5.30036608571 \times 10^{-2}$
30	$2.00560511473 \times 10^{-3}$	$4.57399574759 \times 10^{-2}$	$5.10928394946 \times 10^{-2}$
32	$3.39251992852 \times 10^{-3}$	$4.43591299385 \times 10^{-2}$	$4.93543727896 \times 10^{-2}$
34	$4.53369168047 \times 10^{-3}$	$4.30755529827 \times 10^{-2}$	$4.77620635919 \times 10^{-2}$

Table 10: Three different determinations of the one-loop contribution to $b^{\mathrm{stat}}_{\mathrm{V}}$ with EH static fermions according to the improvement condition eq. (6.13).

L/a	$b^{\mathrm{stat}(1)}_{\mathrm{V,APE}}(\theta=0.0)$	$b^{\mathrm{stat}(1)}_{\mathrm{V,APE}}(\theta=0.5)$	$b^{\mathrm{stat}(1)}_{\mathrm{V,APE}}(\theta=1.0)$
6	$-1.92340408686 \times 10^{-1}$	$7.38125998350 \times 10^{-2}$	$7.32869781736 \times 10^{-2}$
8	$-1.36845655003 \times 10^{-1}$	$6.16212128505 \times 10^{-2}$	$8.47024088104 \times 10^{-2}$
10	$-9.27641005323 \times 10^{-2}$	$5.36113971906 \times 10^{-2}$	$7.11683168091 \times 10^{-2}$
12	$-7.03192609445 \times 10^{-2}$	$4.68591075301 \times 10^{-2}$	$6.11505675084 \times 10^{-2}$
14	$-5.67994367873 \times 10^{-2}$	$4.12586767144 \times 10^{-2}$	$5.32267457567 \times 10^{-2}$
16	$-4.77974262206 \times 10^{-2}$	$3.66636780399 \times 10^{-2}$	$4.69184320708 \times 10^{-2}$
18	$-4.14377364146 \times 10^{-2}$	$3.28289740025 \times 10^{-2}$	$4.17877409334 \times 10^{-2}$
20	$-3.67710201232 \times 10^{-2}$	$2.95586046439 \times 10^{-2}$	$3.75125941270 \times 10^{-2}$
22	$-3.32534218174 \times 10^{-2}$	$2.67170066138 \times 10^{-2}$	$3.38739675354 \times 10^{-2}$
24	$-3.05477831878 \times 10^{-2}$	$2.42109755463 \times 10^{-2}$	$3.07226742530 \times 10^{-2}$
26	$-2.84338924925 \times 10^{-2}$	$2.19744102751 \times 10^{-2}$	$2.79543183872 \times 10^{-2}$
28	$-2.67622184958 \times 10^{-2}$	$1.99587562440 \times 10^{-2}$	$2.54935704579 \times 10^{-2}$
30	$-2.54281229985 \times 10^{-2}$	$1.81272438403 \times 10^{-2}$	$2.32844980335 \times 10^{-2}$
32	$-2.43562070602 \times 10^{-2}$	$1.64513560157 \times 10^{-2}$	$2.12845506743 \times 10^{-2}$
34	$-2.34911031398 \times 10^{-2}$	$1.49085018459 \times 10^{-2}$	$1.94607725049 \times 10^{-2}$

Table 11: Three different determinations of the one-loop contribution to $b^{\mathrm{stat}}_{\mathrm{V}}$ with APE static fermions according to the improvement condition eq. (6.13).

JHEP01(2008)021

(θ_1, θ_2)	β	$c^{\mathrm{stat}}_{\mathrm{V,EH}}$	$c^{\mathrm{stat}}_{\mathrm{V,APE}}$	$c^{\mathrm{stat}}_{\mathrm{V,HYP1}}$	$c^{\mathrm{stat}}_{\mathrm{V,HYP2}}$
(0.0,0.5)	6.0219	0.756(22)	0.478(18)	0.513(18)	0.553(18)
	6.1628	0.577(18)	0.337(14)	0.360(14)	0.409(14)
	6.2885	0.548(17)	0.334(14)	0.359(14)	0.416(14)
	6.4956	0.399(18)	0.240(14)	0.261(14)	0.324(14)
(0.0,1.0)	6.0219	0.707(10)	0.433(8)	0.467(8)	0.508(8)
	6.1628	0.566(8)	0.328(6)	0.352(7)	0.402(7)
	6.2885	0.532(8)	0.318(6)	0.342(6)	0.398(7)
	6.4956	0.406(8)	0.242(7)	0.263(7)	0.327(7)
(0.5,1.0)	6.0219	0.690(8)	0.419(6)	0.452(7)	0.493(6)
	6.1628	0.562(6)	0.325(5)	0.349(5)	0.399(5)
	6.2885	0.527(6)	0.312(5)	0.336(5)	0.392(5)
	6.4956	0.409(6)	0.242(5)	0.264(5)	0.328(5)

Table 12: Non-perturbative determinations of $c_{\mathrm{V}}^{\mathrm{stat}}$ for various gauge couplings and static actions. Different choices of (θ_1, θ_2) correspond to independent definitions of the improvement coefficient.

θ	β	$[Z_{\mathrm{A}}^{\mathrm{stat}}/Z_{\mathrm{V}}^{\mathrm{stat}}]_{\mathrm{EH}}$	$[Z_{\mathrm{A}}^{\mathrm{stat}}/Z_{\mathrm{V}}^{\mathrm{stat}}]_{\mathrm{APE}}$	$[Z_{\mathrm{A}}^{\mathrm{stat}}/Z_{\mathrm{V}}^{\mathrm{stat}}]_{\mathrm{HYP1}}$	$[Z_{\mathrm{A}}^{\mathrm{stat}}/Z_{\mathrm{V}}^{\mathrm{stat}}]_{\mathrm{HYP2}}$
0.0	6.0219	0.9549(13)	0.9611(13)	0.9662(13)	0.9643(13)
	6.1628	0.9564(10)	0.9725(10)	0.9771(9)	0.9785(10)
	6.2885	0.9585(8)	0.9799(9)	0.9837(9)	0.9859(10)
	6.4956	0.9527(7)	0.9823(7)	0.9847(7)	0.9890(6)
0.5	6.0219	0.9549(13)	0.9601(12)	0.9651(12)	0.9633(12)
	6.1628	0.9562(10)	0.9723(10)	0.9769(10)	0.9784(9)
	6.2885	0.9582(8)	0.9796(8)	0.9834(7)	0.9856(9)
	6.4956	0.9528(6)	0.9823(7)	0.9847(6)	0.9890(7)
1.0	6.0219	0.9540(11)	0.9601(11)	0.9651(11)	0.9633(11)
	6.1628	0.9561(9)	0.9723(10)	0.9769(10)	0.9784(8)
	6.2885	0.9583(8)	0.9796(7)	0.9834(7)	0.9856(9)
	6.4956	0.9528(6)	0.9823(6)	0.9847(5)	0.9890(6)

Table 13: Non-perturbative determinations of the O(a)-improved ratio $Z_{\mathrm{A}}^{\mathrm{stat}}/Z_{\mathrm{V}}^{\mathrm{stat}}$ for various gauge couplings and static actions. Different choices of θ correspond to independent definitions of the WI.

θ	β	$(\Delta b_{\rm V}^{\rm stat})_{\rm EH-APE}$	$(\Delta b_{\rm V}^{\rm stat})_{\rm EH-HYP1}$	$(\Delta b_{\rm V}^{\rm stat})_{\rm EH-HYP2}$
0.0	6.0219	0.2177(14)	0.2098(15)	0.2967(18)
	6.1628	0.2122(17)	0.2091(18)	0.2925(21)
	6.2885	0.2130(22)	0.2123(22)	0.2953(26)
	6.4956	0.1869(37)	0.1890(39)	0.2626(11)

θ	β	$(\Delta b_{\rm V}^{\rm stat})_{\rm APE-HYP1}$	$(\Delta b_{\rm V}^{\rm stat})_{\rm APE-HYP2}$	$(\Delta b_{\rm V}^{\rm stat})_{\rm HYP1-HYP2}$
0.0	6.0219	-0.0079(7)	0.0787(10)	0.0865(6)
	6.1628	-0.0031(7)	0.0800(10)	0.0831(6)
	6.2885	-0.0008(8)	0.0820(12)	0.0828(7)
	6.4956	0.0021(11)	0.0756(17)	0.0735(10)

θ	β	$(\Delta b_{\rm V}^{\rm stat})_{\rm EH-APE}$	$(\Delta b_{\rm V}^{\rm stat})_{\rm EH-HYP1}$	$(\Delta b_{\rm V}^{\rm stat})_{\rm EH-HYP2}$
0.5	6.0219	0.2094(18)	0.1987(19)	0.2826(23)
	6.1628	0.2020(24)	0.1983(25)	0.2793(28)
	6.2885	0.2050(28)	0.2018(30)	0.2828(34)
	6.4956	0.1789(51)	0.1777(52)	0.2501(57)

θ	β	$(\Delta b_{\rm V}^{\rm stat})_{\rm APE-HYP1}$	$(\Delta b_{\rm V}^{\rm stat})_{\rm APE-HYP2}$	$(\Delta b_{\rm V}^{\rm stat})_{\rm HYP1-HYP2}$
0.5	6.0219	-0.0106(9)	0.0729(13)	0.0835(7)
	6.1628	-0.0036(10)	0.0771(14)	0.0807(8)
	6.2885	-0.0032(11)	0.0776(15)	0.0808(8)
	6.4956	-0.0004(15)	0.0720(21)	0.0724(12)

θ	β	$(\Delta b_{\rm V}^{\rm stat})_{\rm EH-APE}$	$(\Delta b_{\rm V}^{\rm stat})_{\rm EH-HYP1}$	$(\Delta b_{\rm V}^{\rm stat})_{\rm EH-HYP2}$
1.0	6.0219	0.1332(25)	0.1250(27)	0.2019(34)
	6.1628	0.1301(30)	0.1270(30)	0.2018(34)
	6.2885	0.1391(34)	0.1379(36)	0.2153(41)
	6.4956	0.1284(63)	0.1285(64)	0.2013(68)

θ	β	$(\Delta b_{\rm V}^{\rm stat})_{\rm APE-HYP1}$	$(\Delta b_{\rm V}^{\rm stat})_{\rm APE-HYP2}$	$(\Delta b_{\rm V}^{\rm stat})_{\rm HYP1-HYP2}$
1.0	6.0219	-0.0082(12)	0.0686(19)	0.0768(10)
	6.1628	-0.0030(12)	0.0716(16)	0.0747(8)
	6.2885	-0.0012(13)	0.0761(18)	0.0772(10)
	6.4956	0.0001(17)	0.0728(24)	0.0727(13)

Table 14: Non-perturbative determinations of $\Delta b_{\rm V}^{\rm stat}$ for various gauge couplings and static actions. Different choices of θ correspond to independent improvement conditions.

References

[1] BABAR collaboration, B. Aubert et al., *Measurement of the $B \to \pi l\nu$ branching fraction and determination of $|V(ub)|$ with tagged B mesons*, *Phys. Rev. Lett.* **97** (2006) 211801 [hep-ex/0607089].

[2] CLEO collaboration, N.E. Adam et al., *A study of exclusive charmless semileptonic B decay and $|V_{ub}|$*, *Phys. Rev. Lett.* **99** (2007) 041802 [hep-ex/0703041].

[3] M. Okamoto, *Full determination of the CKM matrix using recent results from lattice QCD*, PoS(LAT2005)013 [hep-lat/0510113].

[4] T. Onogi, *Heavy flavor physics from lattice QCD*, PoS(LAT2006)017 [hep-lat/0610115].

[5] E. Eichten and B.R. Hill, *An effective field theory for the calculation of matrix elements involving heavy quarks*, *Phys. Lett.* **B 234** (1990) 511.

[6] M. Della Morte, A. Shindler and R. Sommer, *On lattice actions for static quarks*, *JHEP* **08** (2005) 051 [hep-lat/0506008].

[7] G.M. de Divitiis, M. Guagnelli, F. Palombi, R. Petronzio and N. Tantalo, *Heavy-light decay constants in the continuum limit of lattice QCD*, *Nucl. Phys.* **B 672** (2003) 372 [hep-lat/0307005].

[8] G.M. de Divitiis, M. Guagnelli, R. Petronzio, N. Tantalo and F. Palombi, *Heavy quark masses in the continuum limit of lattice QCD*, *Nucl. Phys.* **B 675** (2003) 309 [hep-lat/0305018].

[9] D. Guazzini, R. Sommer and N. Tantalo, *$m(b)$ and $f(B/s)$ from a combination of HQET and QCD*, PoS(LAT2006)084 [hep-lat/0609065].

[10] N. Tantalo, *Lattice calculations for B and K mixing*, hep-ph/0703241.

[11] ALPHA collaboration, J. Heitger, M. Kurth and R. Sommer, *Non-perturbative renormalization of the static axial current in quenched QCD*, *Nucl. Phys.* **B 669** (2003) 173 [hep-lat/0302019].

[12] M. Della Morte, P. Fritzsch and J. Heitger, *Non-perturbative renormalization of the static axial current in two-flavour QCD*, *JHEP* **02** (2007) 079 [hep-lat/0611036].

[13] JLQCD collaboration, S. Aoki et al., *$B \to \pi l\bar{\nu}$ form factors with NRQCD heavy quark and clover light quark actions*, *Nucl. Phys.* **83** *(Proc. Suppl.)* (2000) 325 [hep-lat/9911036].

[14] S. Hashimoto, T. Ishikawa and T. Onogi, *Nonperturbative calculation of $Z(A)/Z(V)$ for heavy light currents using Ward-Takahashi identity*, *Nucl. Phys.* **106** *(Proc. Suppl.)* (2002) 352.

[15] Alpha collaboration, R. Frezzotti, P.A. Grassi, S. Sint and P. Weisz, *Lattice QCD with a chirally twisted mass term*, *JHEP* **08** (2001) 058 [hep-lat/0101001].

[16] R. Frezzotti and G.C. Rossi, *Chirally improving Wilson fermions. I: $O(a)$ improvement*, *JHEP* **08** (2004) 007 [hep-lat/0306014].

[17] ALPHA collaboration, F. Palombi, M. Papinutto, C. Pena and H. Wittig, in preparation.

[18] M. Lüscher, *Advanced lattice QCD*, hep-lat/9802029.

[19] R. Sommer, *Non-perturbative QCD: renormalization, $O(a)$-improvement and matching to heavy quark effective theory*, hep-lat/0611020.

[20] M. Lüscher, S. Sint, R. Sommer and P. Weisz, *Chiral symmetry and $O(a)$ improvement in lattice QCD*, *Nucl. Phys.* **B 478** (1996) 365 [hep-lat/9605038].

JHEP01(2008)021

[21] M. Lüscher and P. Weisz, *$O(a)$ improvement of the axial current in lattice QCD to one-loop order of perturbation theory*, *Nucl. Phys.* **B 479** (1996) 429 [hep-lat/9606016].

[22] A. Hasenfratz and F. Knechtli, *Flavor symmetry and the static potential with hypercubic blocking*, *Phys. Rev.* **D 64** (2001) 034504 [hep-lat/0103029].

[23] ALPHA collaboration, M. Kurth and R. Sommer, *Renormalization and $O(a)$-improvement of the static axial current*, *Nucl. Phys.* **B 597** (2001) 488 [hep-lat/0007002].

[24] M. Lüscher, S. Sint, R. Sommer, P. Weisz and U. Wolff, *Non-perturbative $O(a)$ improvement of lattice QCD*, *Nucl. Phys.* **B 491** (1997) 323 [hep-lat/9609035].

[25] F. Palombi, C. Pena and S. Sint, *A perturbative study of two four-quark operators in finite volume renormalization schemes*, *JHEP* **03** (2006) 089 [hep-lat/0505003].

[26] F. Palombi, M. Papinutto, C. Pena and H. Wittig, *A strategy for implementing non-perturbative renormalisation of heavy-light four-quark operators in the static approximation*, *JHEP* **08** (2006) 017 [hep-lat/0604014].

[27] M. Lüscher and P. Weisz, *Efficient numerical techniques for perturbative lattice gauge theory computations*, *Nucl. Phys.* **B 266** (1986) 309.

[28] F. Palombi, R. Petronzio and A. Shindler, *Moments of singlet parton densities on the lattice in the schroedinger functional scheme*, *Nucl. Phys.* **B 637** (2002) 243 [hep-lat/0203002].

[29] C.J. Morningstar and J. Shigemitsu, *Perturbative matching of lattice and continuum heavy-light currents with nrQCD heavy quarks*, *Phys. Rev.* **D 59** (1999) 094504 [hep-lat/9810047].

[30] E. Gabrielli, G. Martinelli, C. Pittori, G. Heatlie and C.T. Sachrajda, *Renormalization of lattice two fermion operators with improved nearest neighbor action*, *Nucl. Phys.* **B 362** (1991) 475.

[31] S. Sint, private notes (1996).

[32] A. Borrelli and C. Pittori, *Improved renormalization constants for B decay and $B\bar{B}$ mixing*, *Nucl. Phys.* **B 385** (1992) 502.

[33] M. Della Morte, R. Hoffmann, F. Knechtli, R. Sommer and U. Wolff, *Non-perturbative renormalization of the axial current with dynamical Wilson fermions*, *JHEP* **07** (2005) 007 [hep-lat/0505026].

[34] ALPHA collaboration, S. Capitani, M. Lüscher, R. Sommer and H. Wittig, *Non-perturbative quark mass renormalization in quenched lattice QCD*, *Nucl. Phys.* **B 544** (1999) 669 [hep-lat/9810063].

[35] M. Lüscher, S. Sint, R. Sommer and H. Wittig, *Non-perturbative determination of the axial current normalization constant in $O(a)$ improved lattice QCD*, *Nucl. Phys.* **B 491** (1997) 344 [hep-lat/9611015].

[36] M. Della Morte et al., *Heavy-strange meson decay constants in the continuum limit of quenched QCD*, arXiv:0710.2201.

[37] S. Sint and P. Weisz, *Further results on $O(a)$ improved lattice QCD to one-loop order of perturbation theory*, *Nucl. Phys.* **B 502** (1997) 251 [hep-lat/9704001].